Research Square

Preprints are preliminary reports that have not undergone peer review.
They should not be considered conclusive, used to inform clinical practice,
or referenced by the media as validated information.

Soliton Dynamics and Stability Analysis in Fractional Modified Kawahara and Landau-Ginzburg-Higgs Models

Myder Jahan Proma
Jamalpur Science & Technology University
Ripan Roy
ripan@usf.edu
University of South Floriada
M. Ali Akbar
University of Rajshahi
Wen-Xiu Ma
University of South Floriada

Article

Keywords: Beta derivative, the new generalized -expansion method, fractional modified Kawahara and Landau-Ginzburg-Higgs models, soliton, stability analysis

Posted Date: November 17th, 2026

DOI: https://doi.org/10.21203/rs.3.rs-11244665/v1

License: This work is licensed under a Creative Commons Attribution 4.0 International License.
Read Full License

Additional Declarations: No competing interests reported.

Soliton Dynamics and Stability Analysis in Fractional Modified Kawahara and Landau-Ginzburg-Higgs Models

Myder Jahan Proma[1], Ripan Roy[1,2,*], M. Ali Akbar[3,4], Wen-Xiu Ma[2,5,6,7*]

[1]Department of Mathematics, Jamalpur Science & Technology University, Bangladesh
[2]Department of Mathematics and Statistics, University of South Florida, Tampa, FL 33620-5700, USA
[3]Department of Applied Mathematics, University of Rajshahi, Bangladesh
[4]Miyan Research Institute, International University of Business Agriculture and Technology, Dhaka, Bangladesh
[5]Department of Mathematics, Zhejiang Normal University, Jinhua 321004, China
[6]Research Center of Astrophysics and Cosmology, Khazar University, 41 Mehseti Street, Baku 1096, Azerbaijan
[7]Material Science Innovation and Modelling, North-West University, Mafikeng Campus, Mmabatho 2735, South Africa

*Correspondence: ripan@usf.edu, wma3@usf.edu

Abstract

In this study, the nonlinear time-fractional modified Kawahara and the space-time fractional Landau-Ginzburg-Higgs models are investigated to explore nonlinear wave propagation in shallow water and higher-order dispersive media with memory effects, as well as nonlocal phase-transition dynamics in superconductors and wave phenomena in plasmas. To transform the governing equations into ordinary differential equations, the appropriate fractional wave transformation called beta-derivative is implemented. By employing the new generalized (G'/G)-expansion method, a broad class of exact analytical solutions is effectively formulated. This procedure yields three separate solution types: hyperbolic, trigonometric, and rational forms. Therefore, a variety of physically relevant wave shapes are derived, including kink, anti-kink, singular soliton, singular periodic, bell-shape, compacton, W-shape, flat parabolic, parabolic, and other types of wave profiles. Additionally, stability analysis is conducted to examine the persistence of the solution. Symbolic calculations and mathematical analysis have been done by Wolfram Mathematica software. The results show that the suggested method is efficient, reliable, and competent for generating a wide variety of intricate nonlinear wave

shapes. Overall, the obtained solutions are essential for comprehending nonlinear wave propagation and the dynamics of complex phenomena in the fields of science and engineering.

Keywords: Beta derivative, the new generalized (G'/G)-expansion method, fractional modified Kawahara and Landau-Ginzburg-Higgs models, soliton, stability analysis.

1. Introduction

Fractional Calculus (FC) is a sophisticated extension of classical calculus which broadens the concepts of differentiation and integration from integer-order processes to include real and complex processes. In recent decades, it has attracted significant interest because of its capability to capture memory and hereditary features, providing more accurate representations than traditional integer-order models [1]. Its numerous applications in plasma physics, control theory [2], charge transfer and stochastic processes [3], optics, and quantum physics [4] demonstrate its significance in capturing complex, nonlocal dynamics. As a result, fractional differential equations have become effective tools for simulating real-world phenomena. Additionally, nonlinear partial differential equations (NPDEs) are essential for describing various nonlinear processes [5], where soliton solutions are particularly significant due to their stability. The increasing relevance of fractional calculus in nonlinear modeling emphasizes the need to develop efficient and accurate analytical techniques. Consequently, the quest for exact traveling wave outcomes of nonlinear fractional differential equations (NFDEs) has emerged as a vital component of modern nonlinear science. Accordingly, a broad spectrum of analytical methods have been suggested in order to create exact and explicit solutions to NFDEs such as the fractional sub-equation method [6], the rational Sine-Gordon expansion method [7], the modified Kudryashov methods [8], Backlund Transformations [9], the homotopy perturbation method [10], unified technique [11], the F-expansion type approach [12], the residual power series method [13], Hirota bilinear form [14].

A wider range of exact traveling wave solutions to various fractional-order nonlinear equations with fixed free parameters is provided by the new generalized (G'/G)-expansion approach, which is a substantial advantage. This technique has been employed to identify solitary wave solutions for various equations, including the fractional Benjamin-Bona-Mahony equation [15] and Kaup-Kupershmidt equation [16], (3+1)-dimensional extended shallow water wave equation [17], Boussinesq model [18], combined KDV-MKDV equation [19], Sharma-Tasso-Olver and Klein-Gordon equations [20]. Exact wave solutions are essential for understanding the internal mechanisms of complicated physical phenomena. It supports initial applications and stability evaluations and helps numerical solvers to confirm the accuracy of their findings. In comparison with existing methods, the proposed approach utilizes simpler algebraic structure and more efficient computational algorithms.

By implementing the new generalized (G'/G)-expansion method, the present study investigates two significant equations to describe the intricate wave structures: the nonlinear time fractional modified Kawahara (TFMK) equation and the space-time fractional Landau-Ginzburg-Higgs (STFLGH) equation. Firstly, the subsequent nonlinear TFMK model is taken into consideration [21]:

$$D_t^{\alpha} v + v^2 v_x + \rho v_{xx} + \tau v_{xxx} = 0, \quad 0 < \alpha \leq 1, \tag{1}$$

where α indicates the fractional order.

The exact wave dynamics and solution structures of KdV-type hierarchies remain a central focus of ongoing mathematical research [22]. The Kawahara problems were first introduced by Kawahara [23] to investigate solitary waves across diverse phenomena in physical science in 1972. In addition to its application in the research of plasma magneto-acoustic waves, this conceptual framework is also utilized in the representation of shallow-water waves that are influenced by surface tension. The TFMK equation is applied in a broad variety of scientific

fields, such as plasma waves and capillary gravitational wave propagation [24]. Various researchers have previously evaluated our preferred TFMK equation. For instance, Guner et al. employed the exp-function method with fractional complex transform and modified Riemann–Liouville derivative to obtain exact solutions to fractional nonlinear equations. They utilized graphical illustrations to verify the effectiveness and behaviour of the solution and derived numerous soliton-type solutions (tanh and exponential forms) for the fractional modified Kawahara and ADR equations [25]. Meanwhile, Topsakal et al. utilized the (G'/G) and $(G'/G, 1/G)$-expansion methods on fractional mBBM and Kawahara equations, employing Jumarie's derivative. They acquired hyperbolic, trigonometric, and rational travelling wave solutions. The results are given in an analytical format; the study does not include any graphical figures [26]. Later, Bashar et al. implemented the advanced $exp(-\phi(\xi))-$ expansion method to study the time-fractional modified Kawahara equation using the conformable fractional derivative. They discovered various exact travelling wave solutions with hyperbolic and trigonometric function structures, such as anti-bright kink, bright bell, dark bell, and lump-shape patterns [27]. Similarly, Shahen et al. examined the conformable time-fractional modified Kawahara equation employing the same advanced $exp(-\phi(\xi))-$expansion technique. They obtained kink, bright-dark bell, and soliton structures, demonstrating the procedure's great efficacy in solving nonlinear problems in mathematical physics [21].

The following nonlinear STFLGH model is considered as the second equation in this study [28]:

$$D_t^{\alpha}(D_t^{\alpha}u) - D_x^{\alpha}(D_x^{\alpha}u) - k^2u + l^2u^3 = 0, \quad 0 < \alpha \leq 1, \tag{2}$$

in this equation, the electrostatic potential of an ion-cyclotron wave is defined by $u = u(x,t)$, where x and t indicate the nonlinear spatial and temporal dimensions, and k, l are real parameters and α is the fractional order of the derivative. The aforementioned equation was

introduced by Landau and Ginzburg to delineate drift cyclotron waves and superconductivity about steady ion-cyclotron waves in nonhomogeneous plasma [29]. Several researchers have explored analytical and numerical solutions of the nonlinear STFLGH equation. Notably, In 2023, Zulqarnain et al. [30] derived new soliton solutions to the space-time fractional Landau-Ginzburg-Higgs equation by applying the truncated M-fractional derivative, where they applied three consistent methods the $(G'/G, 1/G)$-expansion, the modified (G'/G^2)-expansion, and the New Auxiliary Equation Method. Later, Roshid et al. identified several soliton solutions for the truncated time M-fractional Chafee–Infante and Landau–Ginzburg–Higgs models utilizing a unified technique, including kink, lump, and periodic wave patterns [31]. Recently, Abdallah et al. [32] explored the M-fractional Landau–Ginzburg–Higgs equation using modified F-expansion and an enhanced Kudryashov-based unified technique, generating various soliton solutions and examining modulation instability and parameter effects. Around the same time, Ullah et al. employed the modified extended direct algebraic approach with beta derivative to examine the STFLGH problem, through which they discerned several solitary wave solutions, including singular, kink, and periodic solitary waves [28]. Likewise, Mehdi et al. applied Extended Direct Algebraic and Modified F-expansion methods to obtain bright, dark, kink, and anti-kink soliton solutions to the nonlinear LGH problem, as well as investigate bifurcation, chaos, and sensitivity behavior [33]. The STFLGH equation explains mid-latitude and tropical tropospheric nonlinear waves. Rossby waves combine to form these waves, which have long-term connections and restricted dispersion around mid-latitudes and the equator [30]. Diverse disciplines, including condensed matter physics, cosmology, and high-energy physics, have gained insights from NLGHE, facilitating the comprehension of superfluids, superconductors, Bose-Einstein condensates, and the early cosmos, encompassing cosmic string creation [34].

To the best of my knowledge, the new generalized (G'/G)-expansion approach, which is based on β-derivative, has never been used to analyze the TFMK and STFLGH equations before. The absence of investigation of numerous solutions of these equations by implementing this technique, inspired the present investigation. The key purpose of this research is to employ the proposed method to derive exact solutions to the considered nonlinear fractional models and explore their potential applications in nonlinear wave propagation in plasmas and dispersive media with memory effects, and non-local phase-transition dynamics in superconductors. The solutions are represented in trigonometric, hyperbolic and rational function forms under specific conditions.

The subsequent sections of this article are organized as follows: Section 2 contains the requisite preliminaries. Section 3 delineates the new generalized (G'/G)-expansion approach. Section 4 provides innovative and profound analytical solutions for the TFMK and STFLGH equations. Section 5 focuses on the visual depiction and physical analysis of the data using 3D, contour, and 2D plots. Section 6 presents stability analysis. Section 7 demonstrates the comparison of the obtained results with the results of the previous literature. In the final section, the conclusion and future research prospects are presented.

2. Beta derivative

Let $g: [0; 1) \to \mathbb{R}$, then the definition of the β derivative [35] of g is

$$D_t^{\beta}(g) = \lim_{\varepsilon \to 0} \frac{g\left(t+\varepsilon\left(t+\left(\frac{1}{\Gamma(\beta)}\right)\right)\right)^{1-\beta} - g(t)}{\varepsilon}, \ \beta \in (0,1), t > 0 \tag{3}$$

where β denotes the fractional order.

Theorem 1:

Consider $\beta \in (0,1]$ and g and h are β-differentiable functions at a point t, such that the following characteristics are satisfied [19]:

- $D_t^{\beta}(sg(t)+wh(t))=sD_t^{\beta}(g(t))+D_t^{\beta}(h(t)), for, s, w \in \mathbb{R},$
- $D_t^{\beta}(e)=0, for\ e \in \mathbb{R},$
- $D_t^{\beta}(g(t)h(t))=g(t)D_t^{\beta}(h(t))+h(t)D_t^{\beta}(g(t)),$
- $D_t^{\beta}(g(t)/h(t))=g(t)D_t^{\beta}\big(h(t)\big)-h(t)D_t^{\beta}(g(t))/h^2(t),$
- $D_t^{\beta}(g(t))=\left(t+\left(\frac{1}{\Gamma(\beta)}\right)\right)^{1-\beta}(\frac{dg(t)}{dt}).$

Theorem 2:

Let $g: [0; 1) \to \mathbb{R}$ is a function, in which g is a β-differentiable function. Furthermore, consider another differentiable function h, defined within the interval of g. Consequently, we achieve,

$$D_t^{\beta}(g.h)(t)=\left(t+\left(\frac{1}{\Gamma(\alpha)}\right)\right)^{1-\beta}h'(t)g'\big(h(t)\big). \tag{4}$$

The mentioned properties are significant and valuable characteristics of β -derivative [36] and a significant advancement in the fractional derivative has been obtained in [37]. It satisfies all the requirements for classical derivatives as well as strengthens the basis of fractional derivatives.

3. Algorithm of the new generalized (G'/G)-expansion approach

We shall examine a general nonlinear fractional partial differential equation, which can be formulated as:

$$\mathcal{G}\big(v, D_x^{\alpha}v, D_y^{\alpha}v, D_t^{\alpha}v, D_x^{2\alpha}v, D_y^{2\alpha}v, D_t^{2\alpha}v, D_{xy}^{2\alpha}, D_{xt}^{2\alpha}, D_{yt}^{2\alpha}, \dots\big)=0, 0<\alpha\leq 1, \tag{5}$$

where $\mathcal{G}$ be a polynomial of v and $v(x, y, t)=v(\eta)$ is an indeterminate function. The derivatives contain nonlinear elements, and the partial derivatives are denoted by the subscripts x, y, and t in Eq. (5).

Step1: By introducing the traveling-wave transformation, the real variables x, y and t are combined into a compound variable η

$$v(x, y, t)=v(\eta),$$

$$\eta = \frac{\mu}{\alpha}(x + \frac{1}{\Gamma(\alpha)})^{\alpha} + \frac{\theta}{\alpha}(y + \frac{1}{\Gamma(\alpha)})^{\alpha} - \frac{\lambda}{\alpha}(t + \frac{1}{\Gamma(\alpha)})^{\alpha}, \quad (6)$$

The symbols μ, θ represent the wave numbers, whereas the symbol λ represents the velocity of the solitary wave.

Since $v = v(\eta)$, we can implement the transformation Eq. (6) to convert Eq. (5) into an ordinary differential equation:

$$\mathcal{H}(v, v', v'', v''', v^{iv}, v^{v}, \dots) = 0, \quad (7)$$

whereas $\mathcal{H}$ acts as the polynomial of v and its derivatives.

Ordinary derivatives of η are also denoted by primes. Substituting $\theta = 0$ into Eq. (6) yields the following result.

$$v(x, t) = v(\eta),$$
$$\eta = \frac{\mu}{\alpha}(x + \frac{1}{\Gamma(\alpha)})^{\alpha} - \frac{\lambda}{\alpha}(t + \frac{1}{\Gamma(\alpha)})^{\alpha}, \quad (8)$$

Step 2: In this step, equation (7) is integrated as many times as necessary and constants of integration are omitted for simplicity.

Step 3: Subsequently, we establish the solution framework for Eq. (7) as follows:

$$v(\eta) = \sum_{i=0}^{n} c_i (f + \phi)^i + \sum_{i=1}^{n} d_i (f + \phi)^{-i} \quad (9)$$

In Eq. (9), $c_i (i = 0,1,2 \dots \dots, n)$ and $d_i (i = 0,1,2 \dots \dots, n)$

and f be arbitrary constants that will be evaluated later. It retains the condition $c_n = 0, d_n \neq 0$, or $d_n = 0, c_n \neq 0$. But, $c_n = 0$ and $d_n = 0$ are unable to occur at the same time.

The function $\omega(\eta)$ is delineated as follows

$$\phi(\eta) = \frac{G'}{G} \quad (10)$$

wherever $G = G(\eta)$ satisfies the succeeding non-linear equation:

$$MGG'' - NGG' - QG^2 - P(G')^2 = 0 \tag{11}$$

The parameters $M, N, Q\ and\ P$ are considered real, and the dashes signify the standard derivatives with respect to η.

Step 4: To determine the balance number n, we apply the homogeneous balancing approach between the highest-order derivatives and nonlinear terms included in Eq. (7).

Step 5: Modifying Eq. (9) and Eq. (11) to incorporate Eq. (10) into Eq. (7), together with n obtained in Step 4, yields a polynomial in $(f + \phi)^n (n = 0,1,2, \dots)$ and $(f + \phi)^{-n} (n = 0,1,2, \dots)$. Next, a set of algebraic equations is created by equating each coefficient of the derived polynomial to zero for $c_i (i = 0,1,2 \dots \dots, n), d_i (i = 0,1,2 \dots \dots, n), f\ and\ \lambda$.

Step 6: In Step 5, we acquired algebraic equations, and we propose that the values of the constants $c_i (i = 0,1,2 \dots \dots, n), d_i (i = 0,1,2 \dots \dots, n), f\ and\ \lambda$ can be established by solving these equations. Considering the established general solution of Eq. (11), by specifying the parameters $c_i (i = 0,1,2 \dots \dots, n), d_i (i = 0,1,2 \dots \dots, n), f\ and\ \lambda$ in Eq. (9), We derive more comprehensive and innovative exact solutions regarding the nonlinear partial differential equation (5). Applying the generic solution of Eq. (11), we get the succeeding outcomes of Eq. (10):

Family 1: When $N \neq 0$, $\delta = M - P$ and $\omega = N^2 + 4Q(M - P) > 0$

$$\phi(\eta) = \left(\frac{G'}{G}\right) = \frac{N}{2\delta} + \frac{\sqrt{\omega}}{2\delta} \frac{z_1 sinh\left(\frac{\sqrt{\omega}}{2M}\eta\right) + z_2 cosh\left(\frac{\sqrt{\omega}}{2M}\eta\right)}{z_1 cosh\left(\frac{\sqrt{\omega}}{2M}\eta\right) + z_2 sinh\left(\frac{\sqrt{\omega}}{2M}\eta\right)}. \tag{12}$$

Family 2: When $N \neq 0$, $\delta = M - P$ and $\omega = N^2 + 4Q(M - P) < 0$,

$$\phi(\eta) = \left(\frac{G'}{G}\right) = \frac{N}{2\delta} + \frac{\sqrt{-\omega}}{2\delta} \frac{-z_1 sin\left(\frac{\sqrt{-\omega}}{2M}\eta\right) + z_2 cos\left(\frac{\sqrt{-\omega}}{2M}\eta\right)}{z_1 cos\left(\frac{\sqrt{-\omega}}{2M}\eta\right) + z_2 sin\left(\frac{\sqrt{-\omega}}{2M}\eta\right)}. \tag{13}$$

Family 3: When $N \neq 0$, $\delta = M - P$ and $\omega = N^2 + 4Q(M - P) = 0$,

$$\phi(\eta) = \left(\frac{G'}{G}\right) = \frac{N}{2\delta} + \frac{z_2}{z_1 + z_2\eta}. \tag{14}$$

Family 4: When $N = 0$, $\delta = M - P$ and $\xi = \delta Q > 0$,

$$\phi(\eta) = \left(\frac{G'}{G}\right) = \frac{\sqrt{\xi}}{\delta}\frac{z_1 sinh\left(\frac{\sqrt{\xi}}{M}\eta\right) + z_2 cosh\left(\frac{\sqrt{\xi}}{M}\eta\right)}{z_1 cosh\left(\frac{\sqrt{\xi}}{M}\eta\right) + z_2 sinh\left(\frac{\sqrt{\xi}}{M}\eta\right)}. \tag{15}$$

Family 5: When $N = 0$, $\delta = M - P$ and $\xi = \delta Q < 0$,

$$\phi(\eta) = \left(\frac{G'}{G}\right) = \frac{\sqrt{-\xi}}{\delta}\frac{-z_1 sin\left(\frac{\sqrt{-\xi}}{M}\eta\right) + z_2 cos\left(\frac{\sqrt{-\xi}}{M}\eta\right)}{z_1 cos\left(\frac{\sqrt{-\xi}}{M}\eta\right) + z_2 sin\left(\frac{\sqrt{-\xi}}{M}\eta\right)}. \tag{16}$$

4. Application of the new generalized (G'/G)-expansion method

This section employs the new generalized (G'/G)-expansion method to derive exact wave solutions for the nonlinear time-fractional modified Kawahara (TFMK) and space-time fractional Landau-Ginzburg-Higgs (STFLGH) equations.

4.1. The nonlinear TFMK model

A variety of solitary wave forms are obtained by the analysis of the nonlinear TFMK model that is provided in this subsection.

Consider the traveling wave transformation as,

$$\eta = \mu x - \frac{\lambda}{\alpha}(t + \frac{1}{\Gamma(\alpha)})^{\alpha}, \tag{17}$$

By implementing the above transformation (17), the reduced ODE of equation (1) is as follows:

$$-\lambda v' + \mu v^2 v' + \rho\mu^2 v'' + \tau\mu^3 v''' = 0 \tag{18}$$

Integrating Equation (18) with respect to η, we get,

$$-\lambda v + \frac{\mu}{3}v^3 + \rho\mu^2 v' + \tau\mu^3 v'' = 0\,, \tag{19}$$

where $v' = \frac{dv}{d\eta}$.

To obtain the soliton solutions, we balance the term $v''$with the term v^3 in equation (19), resulting in $n = 1$. Hence, we obtain the solution of Eq. (1) as follows:

$$v(\eta) = c_0 + c_1(f + \phi) + d_1(f + \phi)^{-1}, \tag{20}$$

where $c_0, c_1, d_1\ and\ f$ are undetermined constants which need to be computed.

By substituting Eq. (20) along with Eq. (10) and Eq. (11) into Eq. (19), the left side is transformed into a polynomial in $(f+\phi)^i (i = 0,1,2,\dots.)$ and $(f+\phi)^{-i} (i = 0,1,2,\dots.)$. Balancing each coefficient of the resulting polynomial to zero yields a system of algebraic equations for $c_0, c_1, d_1, f and\ \lambda$. To maintain conciseness and simplicity, all algebraic equations have been excluded from this discussion. The subsequent solution sets were derived by resolving this system of equations with Mathematica software.

Set – 1: $f = f, \lambda = -\frac{2\rho^3\left(\pm\frac{1}{\sqrt[3]{(N^2+4\delta Q)}}\right)M}{9\tau^2}, \mu = \frac{\left(\pm\frac{1}{\sqrt[3]{(N^2+4\delta Q)}}\right)\rho M}{\tau},$

$$c_0 = \frac{\left(\pm\frac{2}{\sqrt{-6\tau(N^2+4\delta Q)}}\right)\rho\left(\left(\left(12\delta Q+3N^2\right)\left(\pm\frac{1}{\sqrt[3]{(N^2+4\delta Q)}}\right)\right)-2\delta f-N\right)}{2},$$

$$c_1 = 0, d_1 = \left(\pm\frac{2}{\sqrt{-6\tau(N^2+4\delta Q)}}\right)\rho(\delta f^2 + Nf - Q). \quad (21)$$

Set – 2: $f = f, \lambda = -\frac{2\rho^3\left(\pm\frac{1}{\sqrt[3]{(N^2+4\delta Q)}}\right)M}{9\tau^2}, \mu = \frac{\left(\pm\frac{1}{\sqrt[3]{(N^2+4\delta Q)}}\right)\rho M}{\tau},$

$$c_0 = \frac{\rho\left(\left(\left(12\delta Q+3N^2\right)\left(\pm\frac{1}{\sqrt[3]{(N^2+4\delta Q)}}\right)\right)+2\delta f+N\right)}{3\left(\pm\frac{2}{\sqrt{-6\tau(N^2+4\delta Q)}}\right)\tau(N^2+4\delta Q)}, c_1 = \left(\pm\frac{2}{\sqrt{-6\tau(N^2+4\delta Q)}}\right)\delta\rho, d_1 = 0. \quad (22)$$

Set – 3: $f = \frac{-N}{2\delta}, \lambda = -\frac{2\rho^3\left(\pm\frac{1}{\sqrt[6]{(N^2+4\delta Q)}}\right)M}{9\tau^2}, \mu = \frac{\pm\frac{1}{\sqrt[6]{(N^2+4\delta Q)}}\rho M}{\tau}, c_0 = \frac{\rho\left(\pm\frac{1}{\sqrt[6]{(N^2+4\delta Q)}}\right)}{\tau\left(\pm\frac{1}{\sqrt{-6\tau(N^2+4\delta Q)}}\right)},$

$$c_1 = \pm\frac{\delta\rho}{\sqrt{-6\tau(N^2+4\delta Q)}}, d_1 = -\frac{\rho}{24\delta\tau\left(\pm\frac{1}{\sqrt{-6\tau(N^2+4\delta Q)}}\right)}. \quad (23)$$

Out of the three different sets of solutions, we have decided to proceed with set three for the sake of brevity.

Inserting Eq. (23) into Eq. (20) using Eq. (12) and for the conditions $N \neq 0$, $\delta = M - P$ and $\omega = N^2 + 4Q(M-P) > 0$, we attain the corresponding wave results as ($z_1 \neq 0, z_2 = 0$ and $z_1 = 0, z_2 \neq 0$):

$$v_1(x,t) = \frac{\rho\left(\pm\frac{1}{6\sqrt{(N^2+4\delta Q)}}\right)}{\tau\left(\pm\frac{1}{\sqrt{-(6N^2+24\delta Q)\tau}}\right)} + \frac{\left(\pm\frac{\delta\rho}{\sqrt{-(6N^2+24\delta Q)\tau}}\right)\sqrt{\omega}tanh\left(\frac{\sqrt{\omega}\eta}{2M}\right)}{2\delta} - \frac{\rho}{12\tau\left(\pm\frac{1}{\sqrt{-(6N^2+24\delta Q)\tau}}\right)\sqrt{\omega}tanh\left(\frac{\sqrt{\omega}\eta}{2M}\right)}, \quad (24)$$

where $\eta = \mu x - \frac{\lambda}{\alpha}(t + \frac{1}{\Gamma(\alpha)})^{\alpha}$, $\lambda = -\frac{2\rho^3\left(\pm\frac{1}{6\sqrt{(N^2+4\delta Q)}}\right)M}{9\tau^2}$, which remain unchanged for the remaining wave outcomes (v_2 to v_9) exhibited hereafter.

$$v_2(x,t) = \frac{\rho\left(\pm\frac{1}{6\sqrt{(N^2+4\delta Q)}}\right)}{\tau\left(\pm\frac{1}{\sqrt{-(6N^2+24\delta Q)\tau}}\right)} + \frac{\left(\pm\frac{\delta\rho}{\sqrt{-(6N^2+24\delta Q)\tau}}\right)\sqrt{\omega}coth\left(\frac{\sqrt{\omega}\eta}{2M}\right)}{2\delta} - \frac{\rho}{12\tau\left(\pm\frac{1}{\sqrt{-(6N^2+24\delta Q)\tau}}\right)\sqrt{\omega}coth\left(\frac{\sqrt{\omega}\eta}{2M}\right)}, \quad (25)$$

Likewise, for $N \neq 0$, $\delta = M - P$ and $\omega = N^2 + 4Q(M-P) < 0$, replacing Eq. (23) into Eq. (20) with Eq. (13), the resulting wave solutions ($z_1 \neq 0, z_2 = 0$ and $z_1 = 0, z_2 \neq 0$) are obtained as follows:

$$v_3(x,t) = \frac{\rho\left(\pm\frac{1}{6\sqrt{(N^2+4\delta Q)}}\right)}{\tau\left(\pm\frac{1}{\sqrt{-(6N^2+24\delta Q)\tau}}\right)} - \frac{\left(\pm\frac{\delta\rho}{\sqrt{-(6N^2+24\delta Q)\tau}}\right)\sqrt{-\omega}tan\left(\frac{\sqrt{-\omega}\eta}{2M}\right)}{2\delta} + \frac{\rho}{12\tau\left(\pm\frac{1}{\sqrt{-(6N^2+24\delta Q)\tau}}\right)\sqrt{-\omega}tan\left(\frac{\sqrt{-\omega}\eta}{2M}\right)}, \quad (26)$$

$$v_4(x,t) = \frac{\rho\left(\pm\frac{1}{6\sqrt{(N^2+4\delta Q)}}\right)}{\tau\left(\pm\frac{1}{\sqrt{-(6N^2+24\delta Q)\tau}}\right)} + \frac{\left(\pm\frac{\delta\rho}{\sqrt{-(6N^2+24\delta Q)\tau}}\right)\sqrt{-\omega}cot\left(\frac{\sqrt{-\omega}\eta}{2M}\right)}{2\delta} - \frac{\rho}{12\tau\left(\pm\frac{1}{\sqrt{-(6N^2+24\delta Q)\tau}}\right)\sqrt{-\omega}cot\left(\frac{\sqrt{-\omega}\eta}{2M}\right)}, \quad (27)$$

By applying the conditions $N \neq 0$, $\delta = M - P$, $\omega = N^2 + 4Q(M-P) = 0$ and putting Eq. (23) into Eq. (20) with Eq. (14), we achieve the following wave results as ($z_1 \neq 0, z_2 = 0$ and $z_1 = 0, z_2 \neq 0$):

$$v_5(x,t)=\frac{\rho\left(\pm\frac{1}{6\sqrt{(N^2+4\delta Q)}}\right)}{\tau\left(\pm\frac{1}{\sqrt{-(6N^2+24\delta Q)\tau}}\right)}+\frac{\pm\frac{\delta\rho}{\sqrt{-(6N^2+24\delta Q)\tau}}}{\eta}-\frac{\rho\eta}{24\delta\tau\left(\pm\frac{1}{\sqrt{-(6N^2+24\delta Q)\tau}}\right)}, \tag{28}$$

In the same way, setting the values of Eq. (23) in Eq. (20) with Eq. (15), for $N\neq 0$, $\delta=M-P$ and $\xi=\ \delta Q>0$, yields the following simplified wave solutions for ($z_1\neq 0, z_2=0$ and $z_1=0, z_2\neq 0$):

$$v_6(x,t)=\frac{\rho\left(\pm\frac{1}{6\sqrt{(N^2+4\delta Q)}}\right)}{\tau\left(\pm\frac{1}{\sqrt{-(6N^2+24\delta Q)\tau}}\right)}+\left(\pm\frac{\delta\rho}{\sqrt{-(6N^2+24\delta Q)\tau}}\right)\left(-\frac{N}{2\delta}+\frac{\sqrt{\xi}tanh\left(\frac{\sqrt{\xi}\eta}{M}\right)}{\delta}\right)-$$
$$\frac{\rho}{24\delta\tau\left(\pm\frac{1}{\sqrt{-(6N^2+24\delta Q)\tau}}\right)\left(-\frac{N}{2\delta}+\frac{\sqrt{\xi}tanh\left(\frac{\sqrt{\xi}\eta}{M}\right)}{\delta}\right)}, \tag{29}$$

$$v_7(x,t)=\frac{\rho\left(\pm\frac{1}{6\sqrt{(N^2+4\delta Q)}}\right)}{\tau\left(\pm\frac{1}{\sqrt{-(6N^2+24\delta Q)\tau}}\right)}+\left(\pm\frac{\delta\rho}{\sqrt{-(6N^2+24\delta Q)\tau}}\right)\left(-\frac{N}{2\delta}+\frac{\sqrt{\xi}coth\left(\frac{\sqrt{\xi}\eta}{M}\right)}{\delta}\right)-$$
$$\frac{\rho}{24\delta\tau\left(\pm\frac{1}{\sqrt{-(6N^2+24\delta Q)\tau}}\right)\left(-\frac{N}{2\delta}+\frac{\sqrt{\xi}coth\left(\frac{\sqrt{\xi}\eta}{M}\right)}{\delta}\right)}, \tag{30}$$

Moreover, the substitution of Eq. (23) into Eq. (20) via Eq. (16) results in the following simplified wave outcomes ($z_1\neq 0, z_2=0$ and $z_1=0, z_2\neq 0$) for the conditions $N\neq 0$, $\delta=M-P$ and $\xi=\ \delta Q<0$:

$$v_8(x,t)=\frac{\rho\left(\pm\frac{1}{6\sqrt{(N^2+4\delta Q)}}\right)}{\tau\left(\pm\frac{1}{\sqrt{-(6N^2+24\delta Q)\tau}}\right)}+\left(\pm\frac{\delta\rho}{\sqrt{-(6N^2+24\delta Q)\tau}}\right)\left(-\frac{N}{2\delta}-\frac{\sqrt{-\xi}tan\left(\frac{\sqrt{-\xi}\eta}{M}\right)}{\delta}\right)-$$
$$\frac{\rho}{24\delta\tau\left(\pm\frac{1}{\sqrt{-(6N^2+24\delta Q)\tau}}\right)\left(-\frac{N}{2\delta}-\frac{\sqrt{-\xi}tan\left(\frac{\sqrt{-\xi}\eta}{M}\right)}{\delta}\right)}, \tag{31}$$

$$v_9(x,t) = \frac{\rho\left(\pm\frac{1}{6\sqrt{(N^2+4\delta Q)}}\right)}{\tau\left(\pm\frac{1}{\sqrt{-(6N^2+24\delta Q)\tau}}\right)} + \left(\pm\frac{\delta\rho}{\sqrt{-(6N^2+24\delta Q)\tau}}\right)\left(-\frac{N}{2\delta}+\frac{\sqrt{-\xi}cot\left(\frac{\sqrt{-\xi}\eta}{M}\right)}{\delta}\right) -$$

$$\frac{\rho}{24\delta\tau\left(\pm\frac{1}{\sqrt{-(6N^2+24\delta Q)\tau}}\right)\left(-\frac{N}{2\delta}+\frac{\sqrt{-\xi}cot\left(\frac{\sqrt{-\xi}\eta}{M}\right)}{\delta}\right)}. \quad (32)$$

The unique solutions obtained here are considered a new contribution to this field, which can be very useful for the simulation of nonlinear wave flows in various fields, from shallow water waves described by the TFMK equation to magneto-acoustic phenomena.

4.2. The nonlinear STFLGH model

To reduce the Eq. (2) into an ODE, we assume the traveling wave transformation as:

$$\eta = \frac{\mu}{\alpha}(x+\frac{1}{\Gamma(\alpha)})^{\alpha} - \frac{\lambda}{\alpha}(t+\frac{1}{\Gamma(\alpha)})^{\alpha}, \quad (33)$$

By applying this transformation, Eq. (2) is converted into the following ODE,

$$(\lambda^2-\mu^2)u'' - k^2u + l^2u^3 = 0, \quad (34)$$

where $u' = \frac{du}{d\eta}$.

The balance between the highest nonlinear term $u^3$and the derivative term u''in Eq. (34) produces $n = 1$. Consequently, the solution derivation of Eq. (9) is identical to that of Eq. (20).

By solving the algebraic equation using Mathematica software, we obtained four separate solution sets, which are presented below:

Set – 1: $f = f, \lambda = \pm\frac{\sqrt{-(N^2+4\delta Q)(2k^2M^2-(N^2+4\delta Q)\mu^2)}}{(N^2+4\delta Q)}, \mu = \mu, c_0 = -\frac{(2\delta f+N)k}{\left(\pm\frac{1}{\sqrt{(N^2+4\delta Q)}}\right)l(N^2+4\delta Q)},$

$$c_1 = 0, d_1 = \frac{2\left(\pm\frac{1}{\sqrt{(N^2+4\delta Q)}}\right)(\delta f^2+Nf-Q)k}{l}. \quad (35)$$

Set – 2: $f = f, \lambda = \pm\frac{\sqrt{-(N^2+4\delta Q)(2k^2M^2-(N^2+4\delta Q)\mu^2)}}{(N^2+4\delta Q)}, \mu = \mu, c_0 = -\frac{(2\delta f+N)k}{\left(\pm\frac{1}{\sqrt{(N^2+4\delta Q)}}\right)l(N^2+4\delta Q)},$

$$c_1 = \frac{2\left(\pm\frac{1}{\sqrt{(N^2+4\delta Q)}}\right)\delta k}{l}, d_1 = 0. \tag{36}$$

Set – 3:$f = \frac{-N}{2\delta}, \lambda = \pm\frac{\sqrt{-2(N^2+4\delta Q)\left(k^2M^2-\left((8\delta Q+2N^2)\mu^2\right)\right)}}{2(N^2+4\delta Q)}, \mu = \mu, c_0 = 0,$

$$c_1 = \frac{\left(\pm\frac{1}{\sqrt{(N^2+4\delta Q)}}\right)\delta k}{l}, d_1 = \frac{k}{4\left(\pm\frac{1}{\sqrt{(N^2+4\delta Q)}}\right)\delta l}. \tag{37}$$

Set – 4: $f = \frac{-N}{2\delta}, \lambda = \pm\frac{\sqrt{(N^2+4\delta Q)(k^2M^2+(4\delta Q+N^2)\mu^2)}}{(N^2+4\delta Q)}, \mu = \mu, c_0 = 0, c_1 = \frac{\left(\pm\frac{2}{\sqrt{(-8\delta Q-2N^2)}}\right)\delta k}{l},$

$$d_1 = \frac{k}{2\left(\pm\frac{2}{\sqrt{(-8\delta Q-2N^2)}}\right)\delta l}. \tag{38}$$

Set-3 is the most appropriate result chosen from the aforementioned solutions. The remaining sets are excluded to maintain conciseness and emphasis.

For the conditions $N \neq 0, \delta = M - P$and $\omega = N^2 + 4Q(M-P) > 0$, Eq. (37) is inserted into Eq. (20) along with Eq. (12). After simplification, the subsequent wave outcomes ($z_1 \neq 0, z_2 = 0$ and $z_1 = 0, z_2 \neq 0$) are derived as follows:

$$u_1(x,t) = \frac{\left(\pm\frac{1}{\sqrt{(N^2+4\delta Q)}}\right)k\sqrt{\omega}tanh\left(\frac{\sqrt{\omega}\eta}{2M}\right)}{2l} + \frac{k}{2\left(\pm\frac{1}{\sqrt{(N^2+4\delta Q)}}\right)l\sqrt{\omega}tanh\left(\frac{\sqrt{\omega}\eta}{2M}\right)}, \tag{39}$$

where $\eta = \frac{\mu}{\alpha}(x+\frac{1}{\Gamma(\alpha)})^\alpha - \frac{\lambda}{\alpha}(t+\frac{1}{\Gamma(\alpha)})^\alpha$ and $\lambda = \pm\frac{\sqrt{-2(N^2+4\delta Q)\left(k^2M^2-\left((8\delta Q+2N^2)\mu^2\right)\right)}}{2(N^2+4\delta Q)}$.

These values of η and λ remain same for all the solutions from u_2 to u_9 illustrated below.

$$u_2(x,t) = \frac{\left(\pm\frac{1}{\sqrt{(N^2+4\delta Q)}}\right)k\sqrt{\omega}coth\left(\frac{\sqrt{\omega}\eta}{2M}\right)}{2l} + \frac{k}{2\left(\pm\frac{1}{\sqrt{(N^2+4\delta Q)}}\right)l\sqrt{\omega}coth\left(\frac{\sqrt{\omega}\eta}{2M}\right)}, \tag{40}$$

Similarly, upon applying the conditions $N \neq 0$, $\delta = M - P$ and $\omega = N^2 + 4Q(M-P) < 0$, the substitution of Eq. (37) into Eq. (20) with Eq. (13) yields the following simplified results as ($z_1 \neq 0, z_2 = 0$ and $z_1 = 0, z_2 \neq 0$):

$$u_3(x,t) = -\frac{\left(\pm\frac{1}{\sqrt{(N^2+4\delta Q)}}\right)k\sqrt{-\omega}tan\left(\frac{\sqrt{-\omega}\eta}{2M}\right)}{2l} - \frac{k}{2\left(\pm\frac{1}{\sqrt{(N^2+4\delta Q)}}\right)l\sqrt{-\omega}tan\left(\frac{\sqrt{-\omega}\eta}{2M}\right)}, \tag{41}$$

$$u_4(x,t) = \frac{\left(\pm\frac{1}{\sqrt{(N^2+4\delta Q)}}\right)k\sqrt{-\omega}cot\left(\frac{\sqrt{-\omega}\eta}{2M}\right)}{2l} + \frac{k}{2\left(\pm\frac{1}{\sqrt{(N^2+4\delta Q)}}\right)l\sqrt{-\omega}cot\left(\frac{\sqrt{-\omega}\eta}{2M}\right)}, \tag{42}$$

Incorporating Eqs. (37) and (14) into Eq. (20), we derive the subsequent wave solutions ($z_1 \neq 0, z_2 = 0$ and $z_1 = 0, z_2 \neq 0$) for $N \neq 0$, $\delta = M - P$ and $\omega = N^2 + 4Q(M-P) = 0$:

$$u_5(x,t) = \frac{\left(\pm\frac{1}{\sqrt{(N^2+4\delta Q)}}\right)\delta k}{l\eta} + \frac{k\eta}{4\left(\pm\frac{1}{\sqrt{(N^2+4\delta Q)}}\right)\delta l}, \tag{43}$$

Furthermore, for $N \neq 0$, $\delta = M - P$and $\xi = \delta Q > 0$, placing the values of Eq. (37) into Eq. (20) along with Eq. (15), the resulting wave outcomes ($z_1 \neq 0, z_2 = 0$ and $z_1 = 0, z_2 \neq 0$) are derived as follows:

$$u_6(x,t) = \frac{\left(\pm\frac{1}{\sqrt{(N^2+4\delta Q)}}\right)\delta k\left(-\frac{N}{2\delta}+\frac{\sqrt{\xi}tanh\left(\frac{\sqrt{\xi}}{M}\eta\right)}{\delta}\right)}{l} + \frac{k}{4\left(\pm\frac{1}{\sqrt{(N^2+4\delta Q)}}\right)\delta l\left(-\frac{N}{2\delta}+\frac{\sqrt{\xi}tanh\left(\frac{\sqrt{\xi}}{M}\eta\right)}{\delta}\right)}, \tag{44}$$

$$u_7(x,t) = \frac{\left(\pm\frac{1}{\sqrt{(N^2+4\delta Q)}}\right)\delta k\left(-\frac{N}{2\delta}+\frac{\sqrt{\xi}coth\left(\frac{\sqrt{\xi}}{M}\eta\right)}{\delta}\right)}{l} + \frac{k}{4\left(\pm\frac{1}{\sqrt{(N^2+4\delta Q)}}\right)\delta l\left(-\frac{N}{2\delta}+\frac{\sqrt{\xi}Coth\left(\frac{\sqrt{\xi}}{M}\eta\right)}{\delta}\right)}, \tag{45}$$

By the same approach, for $N \neq 0$, $\delta = M - P$ and $\xi = \delta Q < 0$, we substitute Eq. (37) into Eq. (20) with Eq. (16) and attain the resulting wave outcomes as ($z_1 \neq 0, z_2 = 0$ and $z_1 = 0, z_2 \neq 0$):

$$u_8(x,t) = \frac{\left(\pm\frac{1}{\sqrt{(N^2+4\delta Q)}}\right)\delta k\left(-\frac{N}{2\delta}-\frac{\sqrt{-\xi}\tan\left(\frac{\sqrt{-\xi}}{M}\eta\right)}{\delta}\right)}{l} + \frac{k}{4\left(\pm\frac{1}{\sqrt{(N^2+4\delta Q)}}\right)\delta l\left(-\frac{N}{2\delta}-\frac{\sqrt{-\xi}\tan\left(\frac{\sqrt{-\xi}}{M}\eta\right)}{\delta}\right)} \tag{46}$$

$$u_9(x,t) = \frac{\left(\pm\frac{1}{\sqrt{(N^2+4\delta Q)}}\right)\delta k\left(-\frac{N}{2\delta}+\frac{\sqrt{-\xi}\cot\left(\frac{\sqrt{-\xi}}{M}\eta\right)}{\delta}\right)}{l} + \frac{k}{4\left(\pm\frac{1}{\sqrt{(N^2+4\delta Q)}}\right)\delta l\left(-\frac{N}{2\delta}+\frac{\sqrt{-\xi}\cot\left(\frac{\sqrt{-\xi}}{M}\eta\right)}{\delta}\right)}. \tag{47}$$

The aforementioned various types of exact solutions including hyperbolic, trigonometric, and rational functions are crucial for investigating non-local wave characteristics. These solutions have major significance for modeling the phase transition of superconductors and examining the dynamics of plasma waves and so on.

5. Graphical demonstration and interpretation

A plot is a mathematical or graphical technique that illustrates a data set by depicting the relationship between two or more variables. This section provides graphical representations of results derived from the nonlinear TFMK and STFLGH equations using Mathematica. All derived solutions are stable and explicit, yielding distinct wave profiles based on rational, trigonometric, and hyperbolic functions. The following figures demonstrate three-dimensional, contour, and two-dimensional plots to illustrate these results. Instead of showing discrete data points, three-dimensional wave plots depict how a dependent variable (z) fluctuates with two independent variables (x) and (y). Conversely, a contour plot is a graphical depiction applied to illustrate a three-dimensional surface through constant-z curves projected onto a two-dimensional plane. The wave's gradient, symmetry, and geographical dispersion are shown by

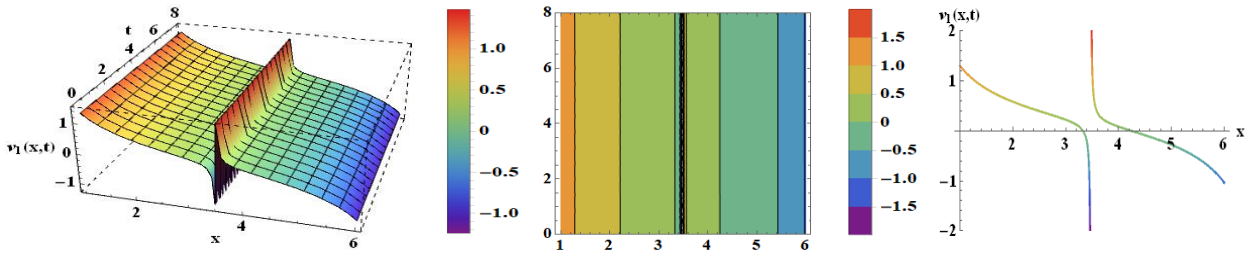
each contour line's equal amplitude. These diagrams are very helpful for finding wave forms' peaks, troughs, and transition zones [19]. In addition, a standard 2D plot comprises two axes, with the independent variable (x) manipulated and the dependent variable (y) observed or measured. These plots illustrate the variation of wave amplitude with a single spatial or temporal variable. By choosing suitable parameter values, different waveforms are generated and analyzed.

5.1. Graphical illustration of the outcomes of the nonlinear TFMK model

Graphical illustrations are employed to investigate the traveling wave solutions from $v_1(x,t)$ to $v_9(x,t)$ of the nonlinear TFMK equation. Three-dimensional surface and contour plots analyze the physical meanings of the solutions, whereas two-dimensional graphs show how the fractional-order derivative affects wave profiles. The solutions presented below encompass a variety of solitary wave forms, including singular soliton, flat parabolic, parabolic, anti-parabolic, singular periodic, anti-kink, kink-shape etc. These results are used to analyze and explain practical phenomena in numerous fields. Parabolic solitons are localized waves with a parabolic amplitude profile on a uniform background used in optical fiber systems for robust high-power pulse transmission [38]. Periodic solitons denote regular waveforms, whereas singular periodic solitons characterize irregular periodic forms, which are valuable for analyzing flux pinning in superconducting materials and intricate oceanic phenomena [39]. In ocean engineering, these discoveries explain how long gravity waves and short wind-generated waves interact. Additionally, they are beneficial for sediment transport, coastal erosion, coastline development, and weather pattern adjustment [40].

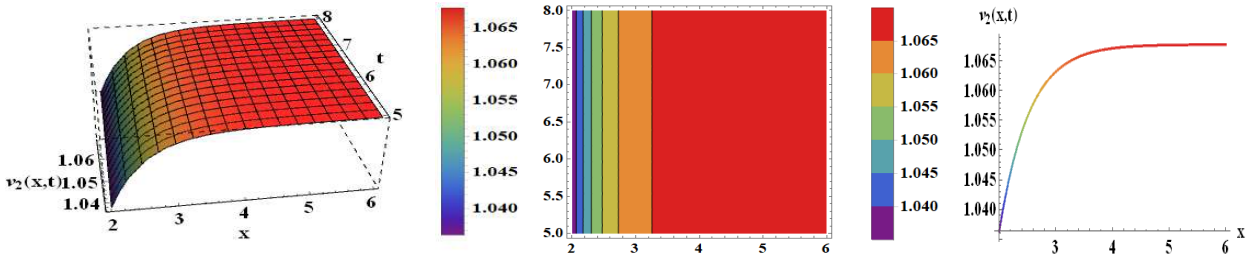
In the following graphs, Fig. 1 illustrates the singular soliton of the solution $v_1(x,t)$ through a 3D surface plot, along with its contour plot, for the parametric values $\mu = 2$, $M = 2.13$, $\delta = 1.056$, $Q = 9.52$, $\rho = 0.39$, $\tau = 0.95$, $N = 1.61$, $\omega = -0.925$, $\alpha = 0.205$, within the region

$1 \leq x \leq 6$ and $0 \leq t \leq 8$ and the associated two-dimensional envelope is portrayed at $t = 1$. In the same manner, the solution $v_2(x,t)$ exhibits a flat parabolic shape soliton for the parameter values $\mu = 1.88$, $M = 2.736$, $\delta = 1.9$, $Q = 9.41$, $\rho = 0.76$, $\tau = -0.1$, $N = 0.506$, $\omega = 8.22$ and fractional order $\alpha = 0.99$, within the region $2 \leq x \leq 6$, $5 \leq t \leq 8$ depicted in Fig. 2, with the corresponding 2D spatial profile at $t = 5$. Again, for the parameter values $\mu = 0.69$, $M = 2.12$, $\delta = 0.725$, $Q = -2$, $\rho = 1.29$, $\tau = -0.1$, $N = 2.908$, $\omega = -2$ and fractional order $\alpha = 0.99746$, within the region $2 \leq x \leq 6$, $2 \leq t \leq 4$, Fig. 3 demonstrates a parabolic shape soliton structure of $v_3(x,t)$ accompanied by its 2D projection at $t = 2$.



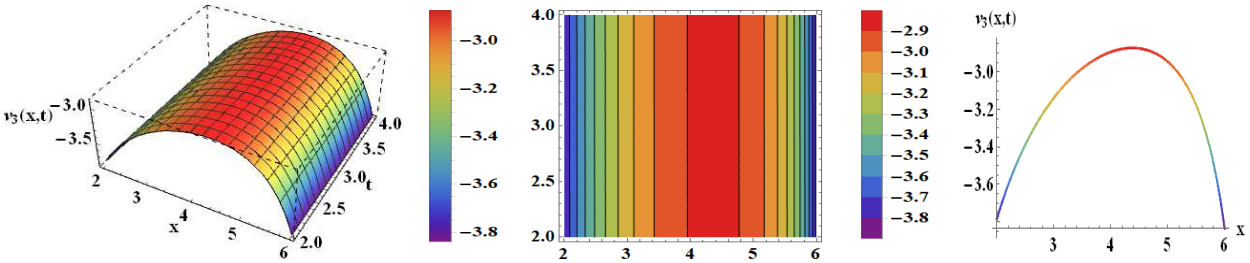
(a) 3D Profile **(b) Contour Profile** **(c) 2D Profile**

Fig. 1: Graphical visualization of the soliton solution $v_1(x,t)$



(a) 3D Profile **(b) Contour Profile** **(c) 2D Profile**

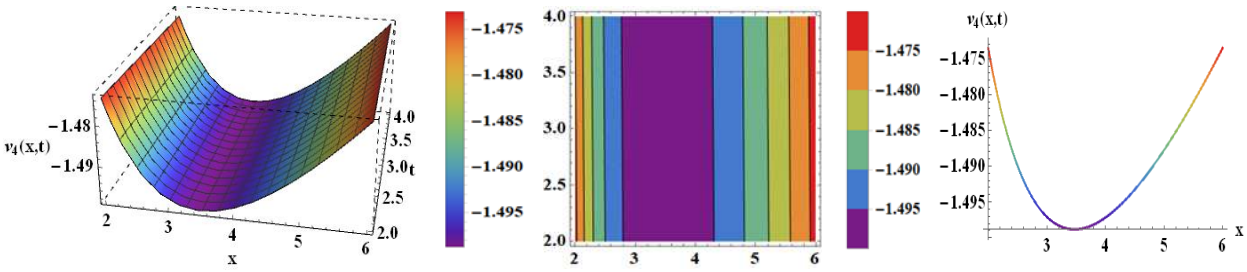
Fig. 2: Graphical visualization of the soliton solution $v_2(x,t)$



(a) 3D Profile **(b) Contour Profile** **(c) 2D Profile**

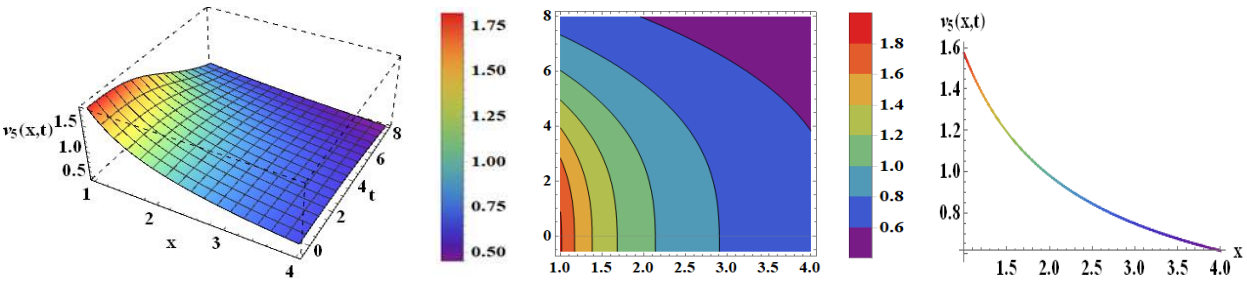
Fig. 3: Graphical visualization of the soliton solution $v_3(x,t)$

Similarly, Fig. 4 portrays the anti-parabolic shape profile of the solution $v_4(x,t)$ for the parameter values $\mu = 0.055$, $M = 2.12$, $\delta = -0.1$, $Q = -2$, $\rho = 1.29$, $\tau = -0.1$, $N = 2$, $\omega = -2$ and $\alpha = 0.99746$. The solution is depicted over the boundary $2 \leq x \leq 6$, $2 \leq t \leq 4$, while the corresponding 2D plot highlights the spatial profile at $t = 2$. Moreover, we obtain the general soliton structure of $v_5(x,t)$ for the parametric values $\mu = 0.25$, $M = 0.52$, $\delta = 1.79$, $Q = 0.25$, $\rho = 0.755$, $\tau = 0.84$, $N = 0.878$, $\alpha = 2.865$, within the region $1 \leq x \leq 4$, $-1 \leq t \leq 8$ along with its 2D spatial profile for $t = 3$ demonstrated in Fig. 5. Likewise, Fig. 6 portrays the anti-kink shaped soliton of solution $v_6(x,t)$ for the values $\mu = -1.04$, $M = 0.7$, $\delta = -3$, $Q = -1.32$, $\rho = 2.405$, $\tau = 1.28$, $N = -2.29$, $\xi = 0.155$ and $\alpha = 0.9$, over the region $-10 \leq x \leq 10$, $-1 \leq t \leq 10$ and the corresponding 2D spatial profile shown at $t = 1$.



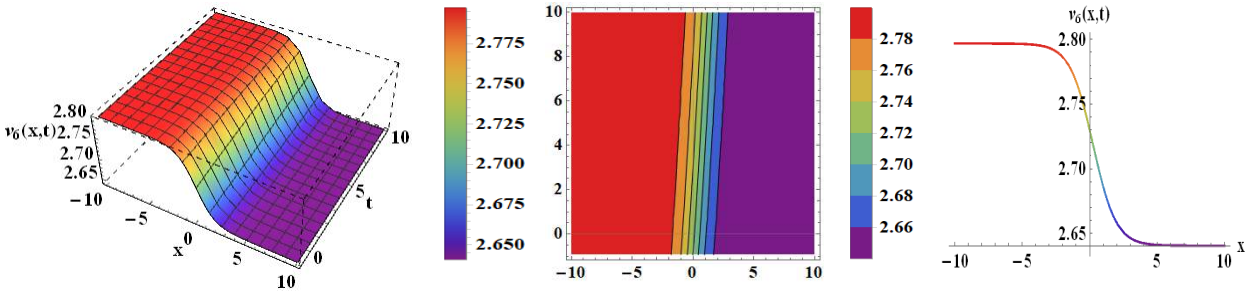
(a) 3D Profile **(b) Contour Profile** **(c) 2D Profile**

Fig. 4: Graphical visualization of the soliton solution $v_4(x,t)$



(a) 3D Profile **(b) Contour Profile** **(c) 2D Profile**

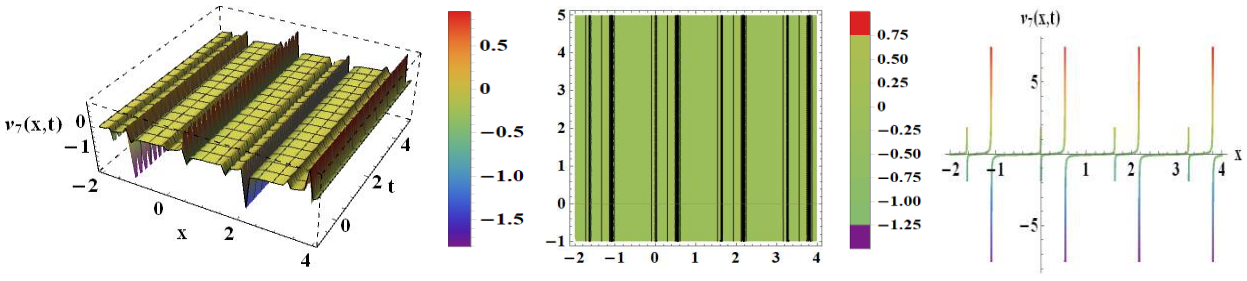
Fig. 5: Graphical visualization of the soliton solution $v_5(x,t)$



(a) 3D Profile **(b) Contour Profile** **(c) 2D Profile**

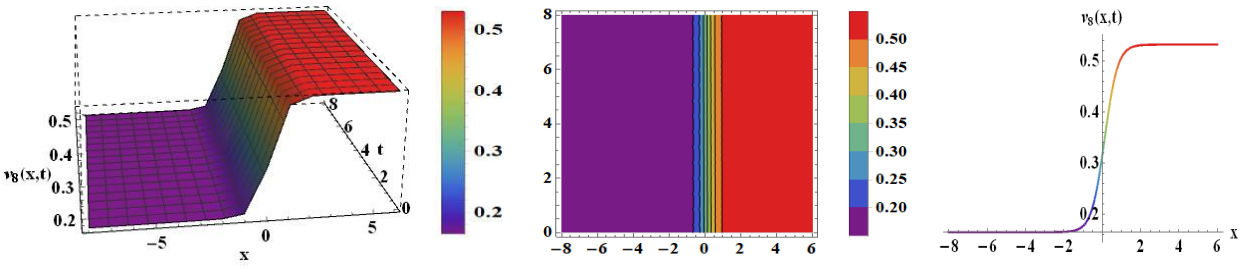
Fig. 6: Graphical visualization of the soliton solution $v_6(x,t)$

In a similar manner, the solution $v_7(x,t)$ characterizes the singular periodic shape for the parametric values $\mu = 2.0,\ M = 1.47,\ \delta = 1.552,\ Q = 7.17,\ \rho = -0.1,\ \tau = 1.705,\ N = 0.705,\ \xi = -2,\ \alpha = 0.9777$, within the region $-2 \le x \le 4, -1 \le t \le 5$, with the respective 2D spatial profile at $t = 1$, illustrated in Fig. 7. Again, for the parameter values $\mu = 2.0,\ M = 1,\ \delta = 2.0,\ Q = 1,\ \rho = 0.9,\ \tau = 0.9,\ N = 0.9,\ \xi = 0.59$,$\alpha = 0.9$, the solution $v_8(x,t)$ signifies the smooth kink shape portrayed in Fig. 8 within the boundary $-8 \le x \le 6, 0 \le t \le 8$ along with its spatial 2D projection at $t = 1$. Furthermore, Fig. 9 demonstrates the kink shaped structure of the solution $v_9(x,t)$ over the domain $1 \le x \le 7,\ 1 \le t \le 10$, with its corresponding 2D spatial profile at $t = 1$ for the parametric values $\mu = -0.71,\ M = 2.8,\ \delta = 3.8,\ Q = 5.45,\ \rho = 0.65,\ \tau = 0.179,\ N = -0.6,\ \xi = -2.895$ and fractional order $\alpha = 0.89$.



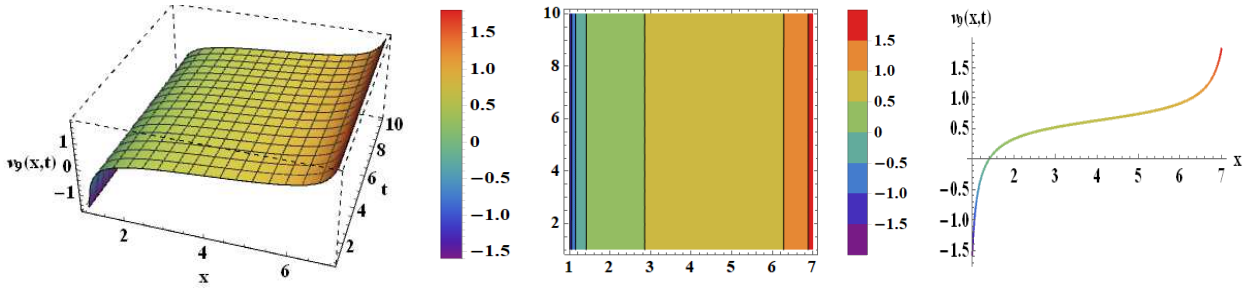
(a) 3D Profile **(b) Contour Profile** **(c) 2D Profile**

Fig. 7: Graphical visualization of the soliton solution $\mathbf{v_7(x,t)}$



(a) 3D Profile **(b) Contour Profile** **(c) 2D Profile**

Fig. 8: Graphical visualization of the soliton solution $v_8(x,t)$



(a) 3D Profile **(b) Contour Profile** **(c) 2D Profile**

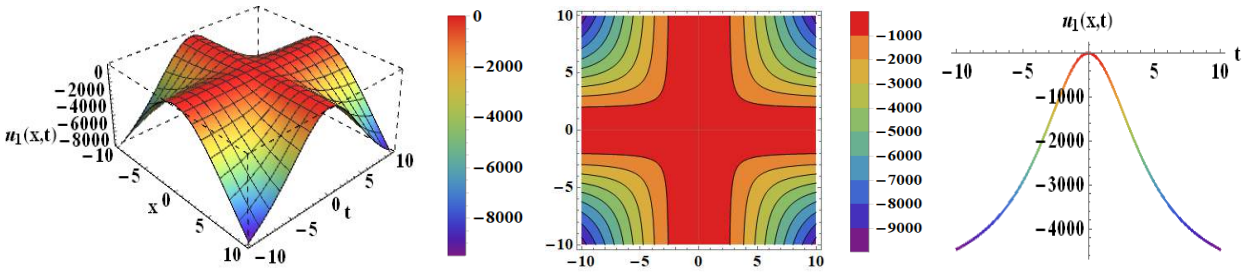
Fig. 9: Graphical visualization of the soliton solution $v_9(x,t)$

5.2. Graphical illustration of the outcomes of the nonlinear STFLGH model

A wide range of soliton solutions, from $u_1(x,t)$ to $u_9(x,t)$ are obtained from the nonlinear STFLGH equation which involves a number of unknown parameters. These solutions exhibit several kinds of wave forms by assigning a variety of particular values to the unknown parameters including parabolic shape, W-shape, bell shape, kink, anti-kink, compacton etc. Solitons retain their identity after encounters with other solitons. Soliton solutions feature cosmic strings, domain walls, and particle-like magnetic monopoles, which are crucial to early universe cosmology [41]. Bell-shaped solitons prevent dispersion, preserve pulse integrity, and reduce errors in optical fiber communications, making them vital for high-capacity, long-distance, and complex systems [42]. In shallow waters, kink and anti-kink solitons are localized depressions and disturbances that simulate solitary waves and inverse solitary waves, respectively [39]. The characterization of plasma properties and the analysis of signal transmission in optical fibers could potentially be aided by the acquired solutions [43]. They

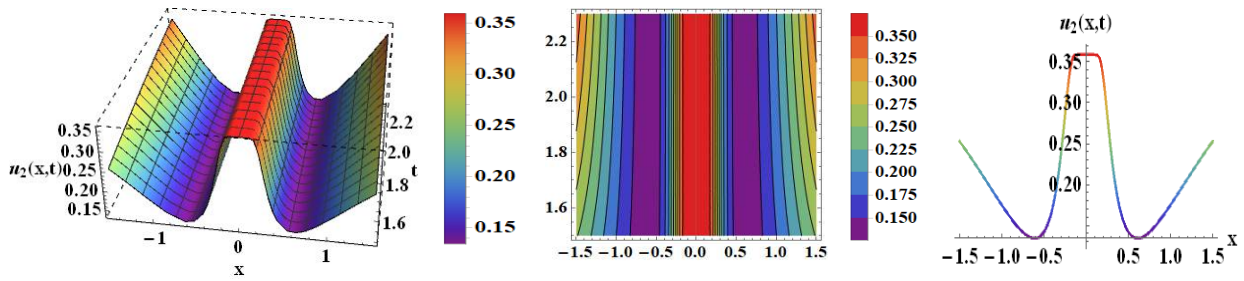
also play a major role in solid-state physics, nonlinear optics, ion sound waves in plasma, oscillations in a nonlinear string, hydro-magnetic waves in cold plasma [44] and so on.

The solution $u_1(x,t)$ exhibits a general soliton structure for the parameter values $\mu = -0.2$, $M = -0.554$, $\delta = -3$, $Q = -0.9$, $k = 1.5$, $l = 2.5$, $N = -1.5$, $\omega = 0.08$ and $\alpha = -2.0$ in the spatial and temporal domains $-10 \le x \le 10$ and $-10 \le t \le 10$, with the corresponding 2D temporal profile shown at $x = 6$. Subsequently, Fig. 2 illustrates the graphical representation of the W-shape soliton structure of the solution $u_2(x,t)$ under the parameter values $\mu = -0.2$, $M = -0.554$, $\delta = -3$, $Q = -0.9$, $k = -0.335$, $l = 2.5$, $N = -1.5$, $\omega = 0.49$ and $\alpha = -2.0$. The solution is shown in the spatial and temporal domains of $-1.5 \le x \le 1.5$ and $1.5 \le t \le 2.3$, with the corresponding 2D spatial profile shown at $t = 1.5$. Again, for the parameter values $\mu = -1.82$, $M = -5$, $\delta = -3$, $Q = -0.9$, $k = 1.5$, $l = 2.5$, $N = -1.5$, $\omega = 0.49$ and $\alpha = -2.0$, the solution $u_3(x,t)$ yields parabolic shape as depicted in Fig. 3, within $-1.5 \le x \le 1.5$ and $1.5 \le t \le 2.3$, with the 2D spatial profile shown at $t = 2$.



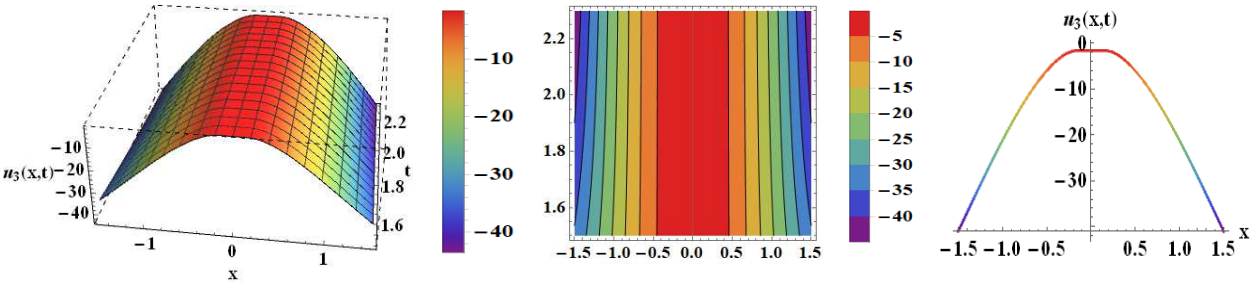
(a) 3D Profile **(b) Contour Profile** **(c) 2D Profile**

Fig. 10: Graphical visualization of the soliton solution $u_1(x,t)$



(a) 3D Profile **(b) Contour Profile** **(c) 2D Profile**

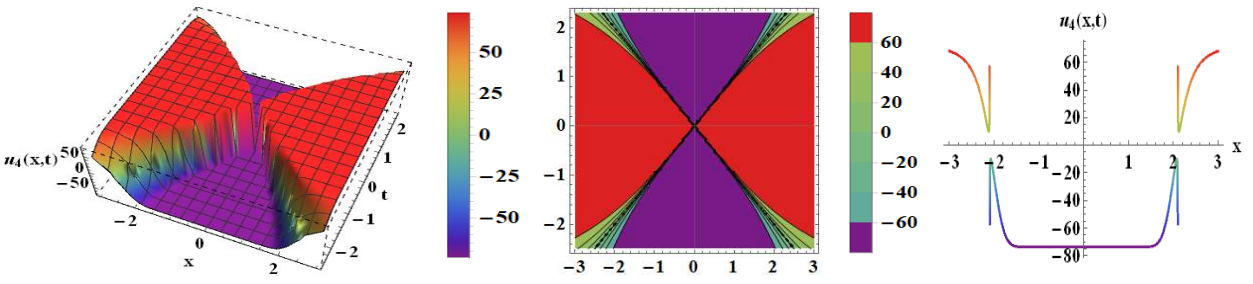
Fig. 11: Graphical visualization of the soliton solution $u_2(x,t)$



(a) 3D Profile **(b) Contour Profile** **(c) 2D Profile**

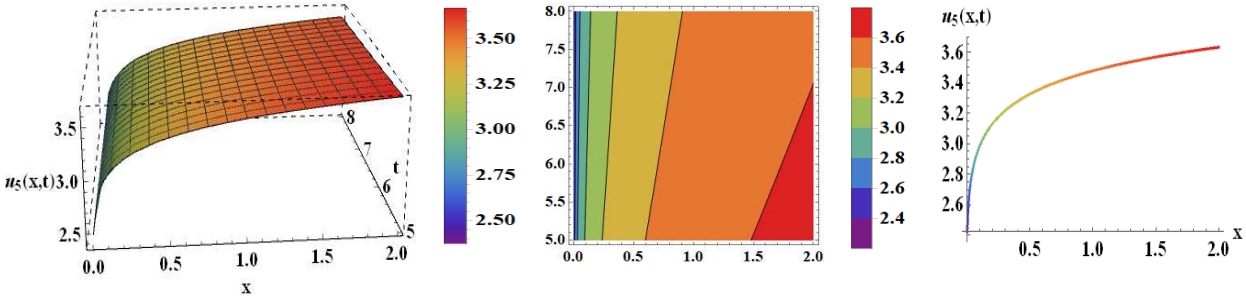
Fig. 12: Graphical visualization of the soliton solution $u_3(x,t)$

Similarly, Fig. 4 depicts a singular soliton form of solution $u_4(x,t)$, for the parametric values $\mu = 5.64$, $M = -0.045$, $\delta = -3.6$, $Q = -2.0$, $k = -0.98$, $l = 0.1$, $N = -4$, $\omega = 0.2$ and $\alpha = -2.0$. The solution is shown in the spatial and temporal domains of $-3 \leq x \leq 3$ and $-2.5 \leq t \leq 2.3$, with the corresponding 2D spatial profile shown at $t = -2.1$. Furthermore, the solution $u_5(x,t)$ produces a flat parabolic shape soliton for $\mu = 1.49$, $M = 3$, $\delta = 2.8$, $Q = 0.3$, $k = -1.19$, $l = -2.38$, $N = 2.82$ and fractional order $\alpha = 0.008$, within the boundary $0 \leq x \leq 2$ and $5 \leq t \leq 8$, while the corresponding 2D spatial profile is shown at $t = 6$. Likewise, Fig. 6 portrays a smooth kink shape of solution $u_6(x,t)$ for the parametric values $\mu = 2.205$, $M = 1.245$, $\delta = 1.953$, $Q = 10$, $k = 1.924$, $l = 0.854$, $N = 1.81$, $\xi = 1.475$ and $\alpha = 0.82$ in the region $1.5 \leq x \leq 5$ and $-2 \leq t \leq 8$, with the corresponding 2D profile shown for $x = 3$.



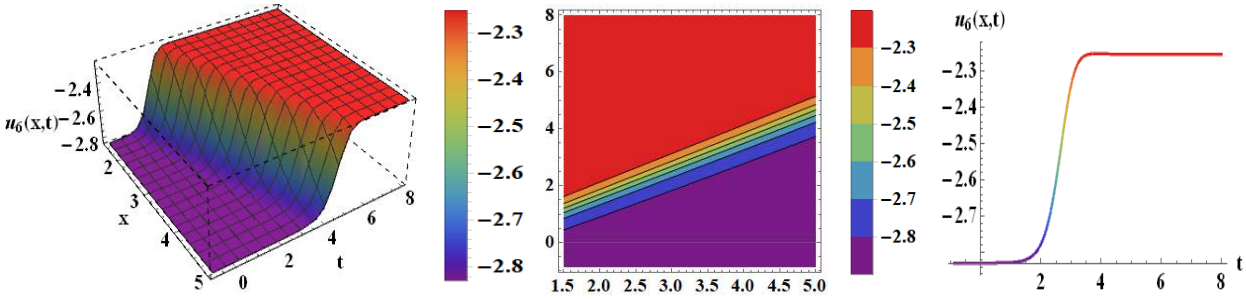
(a) 3D Profile **(b) Contour Profile** **(c) 2D Profile**

Fig. 13: Graphical visualization of the soliton solution $u_4(x,t)$



(a) 3D Profile **(b) Contour Profile** **(c) 2D Profile**

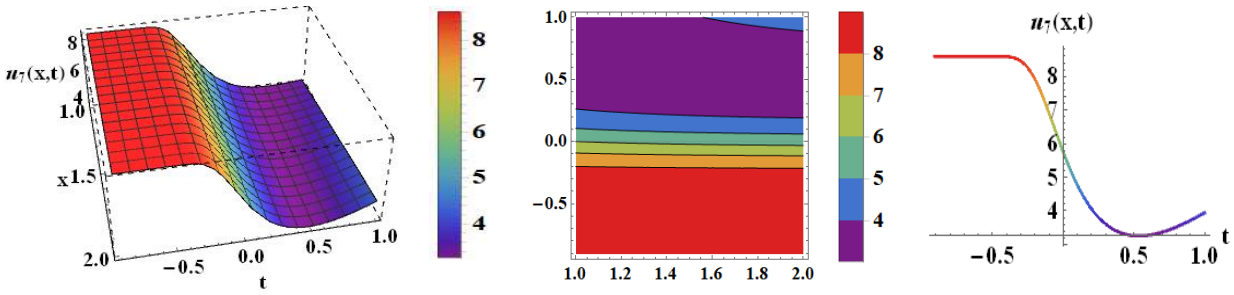
Fig. 14: Graphical visualization of the soliton solution $u_5(x,t)$



(a) 3D Profile **(b) Contour Profile** **(c) 2D Profile**

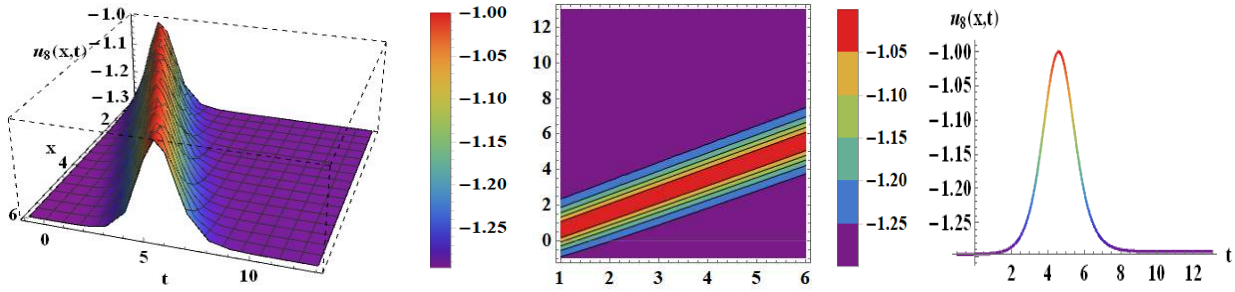
Fig. 15: Graphical visualization of the soliton solution $u_6(x,t)$

Again, for a different set of parameter values $\mu = -1.05$, $M = 0.31$, $\delta = 0.95$, $Q = 10$, $k = 2.0$, $l = 0.615$, $N = 1.68$, $\xi = 1.92$ and $\alpha = -3.16$ within the range $1 \leq x \leq 2$ and $-0.91 \leq t \leq 1$, Fig. 7 illustrates anti-kink shape of the solution $u_7(x,t)$, with the 2D temporal profile shown at $x = 1.5$. Moreover, for solution $u_8(x,t)$, a bell shape profile is obtained within the boundary $1 \leq x \leq 6$ and $-1 \leq t \leq 13$, for the parametric values $\mu = 2.175$, $M = 2.925$, $\delta = 1.492$, $Q = 1.32$, $k = 0.1$, $l = 0.1$, $N = 2.0$, $\xi = 2.0$, $\alpha = 0.916$, with the 2D temporal profile shown for $x = 5$ depicted in Fig. 8. Additionally, a compacton soliton shape is illustrated in Fig. 9 for the solution $u_9(x,t)$ in the spatial and temporal domains of $3.1 \leq x \leq 3.5$ and $2.1 \leq t \leq 2.5$, accompanied by its 2D spatial profile shown at $t = 2.1$, for the parametric values $\mu = -0.75$, $M = 2.8$, $\delta = 3.56$, $Q = 4.75$, $k = 0.179$, $l = 0.65$, $N = -0.6$, $\xi = -3$ and $\alpha = 0.89$.



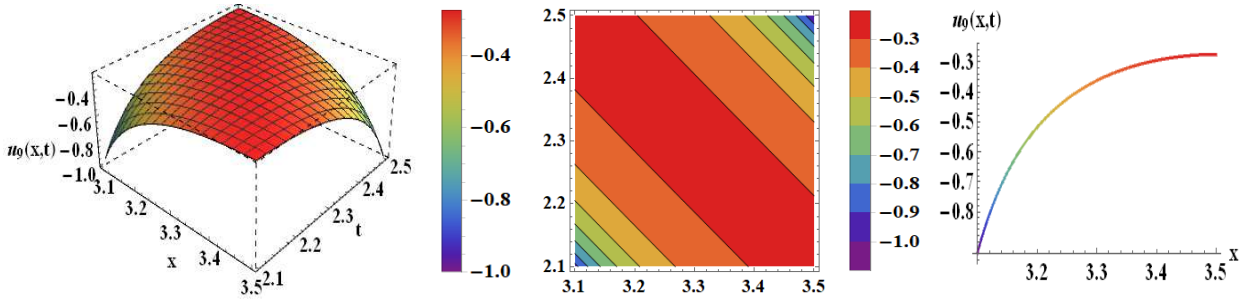
(a) 3D Profile **(b) Contour Profile** **(c) 2D Profile**

Fig. 16: Graphical visualization of the soliton solution $u_7(x,t)$



(a) 3D Profile **(b) Contour Profile** **(c) 2D Profile**

Fig. 17: Graphical visualization of the soliton solution $u_8(x,t)$



(a) 3D Profile **(b) Contour Profile** **(c) 2D Profile**

Fig. 18: Graphical visualization of the soliton solution $u_9(x,t)$

6. Stability Analysis

Stability analysis is widely used to determine the stable or unstable behavior of nonlinear systems under slight perturbations. In nonlinear wave dynamics, linear stability analysis is important for examining the persistence of wave solutions during propagation. This method investigates the response of the system to infinitesimal disturbances and identifies the parameter regions where the solutions remain stable and bounded. In this section, the stability

behaviour of the nonlinear TFMK equation and the nonlinear STFLGH equation is analyzed using the linear stability technique.

6.1. The stability analysis of the TFMK model

The perturbed solution to the governing model (1) is formulated as

$$v = v_0 + \varepsilon V(x,t), \tag{48}$$

where v_0 signifies the equilibrium solution of the governing equation, ε indicates a minor perturbation parameter, and $V(x,t)$ denotes the perturbed wave solution. Inserting the above Eq. (48) into Eq. (1), we get the linearizing form as follows:

$$D_t^{\alpha} V + {v_0}^2 V_x + \rho V_{xx} + \tau V_{xxx} = 0 \tag{49}$$

To solve Eq. (49), we consider the following solution:

$$V(x,t) = e^{i\left(\mu x - \frac{\lambda}{\alpha}(t+\frac{1}{\Gamma(\alpha)})^{\alpha}\right)} \tag{50}$$

In order to solve for λ, we insert Eq. (50) into Eq. (49) and obtain the following result:

$$\lambda = \mu {v_0}^2 + i\mu^2\rho - \mu^3\tau \tag{51}$$

The real and imaginary components of λ are

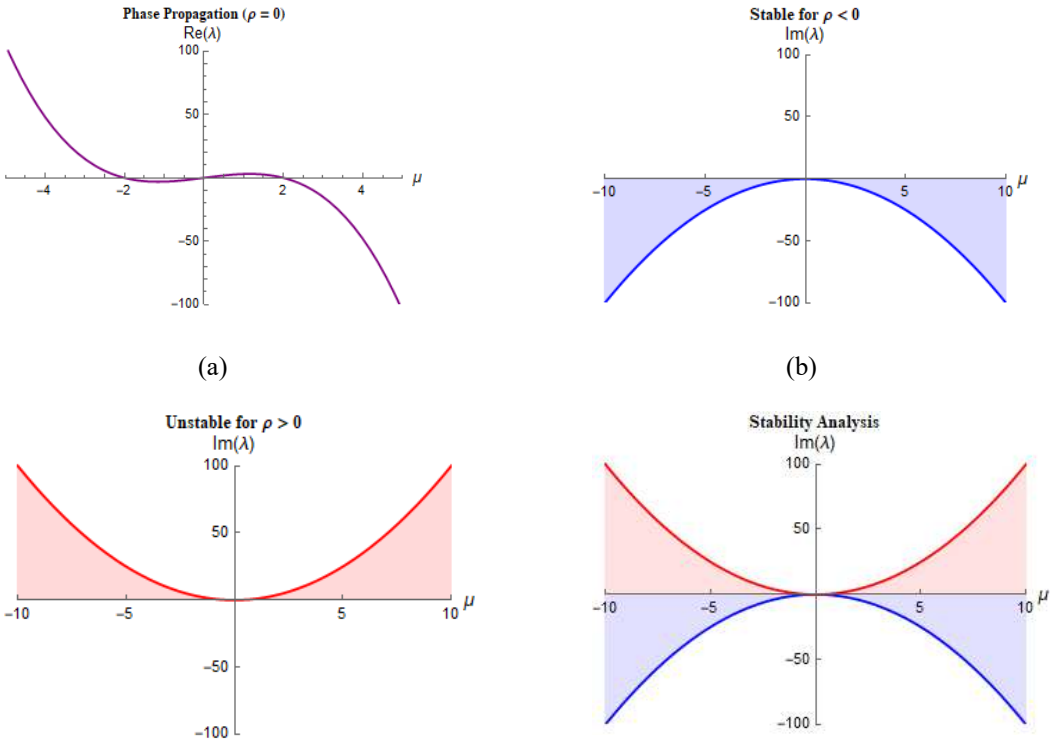
$$Re\ (\lambda) = \mu {v_0}^2 - \mu^3\tau \text{ and } Im\ (\lambda) = \mu^2\rho$$

The real component of λ dictates the oscillatory behaviour (phase propagation) of the perturbation illustrated in Fig. 19(a), while the imaginary component governs the temporal growth or decay of the perturbation amplitude as depicted in Fig 19(b) - 19(d).

(i) Stable for $Im\ (\lambda) < 0$ (if $\rho < 0$): The system will be stable when the perturbation decays exponentially.

(ii) Unstable for $Im\ (\lambda) > 0$ (if $\rho > 0$): The system will be unstable when the perturbation amplitude grows exponentially.

(iii) Neutrally Stable for $Im\ (\lambda) = 0$ (if $\rho = 0$): As illustrated in Fig. 19(a), the perturbation amplitude remains constant, reducing system dynamics to pure wave propagation.



(a) (b)

(c) (d)

Fig. 19: Stability analysis of Eq. (1)

6.2. The stability analysis of the STFLGH model

The perturbed form of the solution to the governing model (2) is denoted as

$$u = u_0 + \varepsilon U(x,t) \tag{52}$$

We obtain the following linear differential equation, by substituting the perturbed wave solution (52) into Eq. (2):

$$D_t^{\alpha}(D_t^{\alpha}U) - D_x^{\alpha}(D_x^{\alpha}U) - k^2U + 3l^2{u_0}^2U = 0 \tag{53}$$

To solve Eq. (53), we utilize a solution consistent with its characteristic form,

$$U(x,t) = e^{i\left(\frac{\mu}{\alpha}(x+\frac{1}{\Gamma(\alpha)})^{\alpha} - \frac{\lambda}{\alpha}(t+\frac{1}{\Gamma(\alpha)})^{\alpha}\right)}, \tag{54}$$

where, μ and λ symbolize the perturbed wave number and phase velocity.

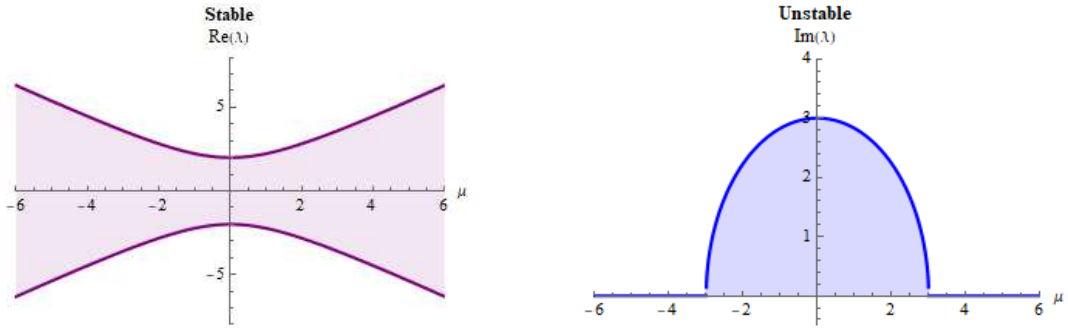
Employing Eq. (54) and its derivatives in Eq. (53) and solving for λ, we obtain as follows:

$$\lambda = \sqrt{\mu^2 + 3l^2{u_0}^2 - k^2} \tag{55}$$

The stability of the steady-state solution is controlled by the characteristics of the discriminant within the radical, which influences the behaviour of the perturbation profile.

(i) Stable for $\mu^2 + 3l^2{u_0}^2 > k^2$: The perturbation is a bounded harmonic oscillation when the discriminant is positive. Steady-state solution is stable because disturbance amplitude does not change over time as illustrated in Fig. 20(a).

(ii) Unstable for $\mu^2 + 3l^2{u_0}^2 < k^2$: The perturbation amplitude grows exponentially with a negative discriminant, causing modulational instability and wave structure destabilization as depicted in Fig. 20(b).



(a) (b)

Fig. 20: Stability analysis Eq. (2)

7. Comparison and discussion

To investigate the distinctiveness of this study, we have compared the accomplished results of the nonlinear TFMK and STFLGH equations with the outcomes attained by Bashar et al. [27], and Singh et al. [45], in Tables 1-2 respectively.

7.1. Comparative investigation of solutions to the nonlinear TFMK model

Many researchers have earlier utilized several methodologies to get numerous analytical solutions for the nonlinear TFMK equation. In this study, this equation is analyzed by implementing the new generalized (G'/G)-expansion procedure with the help of beta-

derivative. Several forms of solutions are derived based on the values assigned to the nonlinearity parameters. Bashar et al. [27] analyzed the same equation by means of the advanced $exp(-\phi(\xi))$ −expansion method and presented the solutions mainly in two types which are hyperbolic and trigonometric functions. They were unable to generate rational solutions as a result of undefined coefficients when establishing specific parameters, which led to the omission of those cases. In contrast, the present method has obtained three kinds of soliton solutions derived from hyperbolic, trigonometric and rational functions as shown in Table 1. Additionally, 3D, contour and 2D plots are depicted to explain the dynamical behaviour of parabolic, anti-parabolic, flat parabolic shape, singular kink shaped, kink shaped, anti-kink shaped, and periodic solitons. Stability analysis is also performed in this study. Therefore, these outcomes demonstrate a richer wave structure and validate the uniqueness of this study.

Table 1: Comparison of the obtained solutions with the solutions identified by Bashar et al. [27].

Obtained solutions in this study	Solutions obtained by Bashar et al. [27]
1. The hyperbolic function solution is $v_1(x,t) = \frac{\rho\left(\pm\frac{1}{6\sqrt{(N^2+4\delta Q)}}\right)}{\tau\left(\pm\frac{1}{\sqrt{-(6N^2+24\delta Q)\tau}}\right)} + \frac{\left(\pm\frac{\delta\rho}{\sqrt{-(6N^2+24\delta Q)\tau}}\right)\sqrt{\omega}tanh\left(\frac{\sqrt{\omega}\eta}{2M}\right)}{2\delta} - \frac{\rho}{12\tau\left(\pm\frac{1}{\sqrt{-(6N^2+24\delta Q)\tau}}\right)\sqrt{\omega}tanh\left(\frac{\sqrt{\omega}\eta}{2M}\right)}$, where $\eta = \mu x - \frac{\lambda}{\alpha}(t+\frac{1}{\Gamma(\alpha)})^{\alpha}, \lambda = -\frac{2\rho^3\left(\pm\frac{1}{6\sqrt{(N^2+4\delta Q)}}\right)M}{9\tau^2}$, and μ is a constant.	1.The hyperbolic function solution is $u_{1,2}(x,t) = \frac{\alpha}{6}\sqrt{-\frac{6}{\beta}} \pm \frac{1}{6}\frac{\alpha\sqrt{-\frac{6}{\beta}}}{\sqrt{-\frac{1}{\lambda\mu}}\mu\sqrt{\frac{-\lambda}{\mu}}tanh\left(\sqrt{-\lambda\mu}(\xi+C)\right)}$, where $\xi = \pm\frac{\sqrt{-\frac{1}{36\lambda\mu}}\alpha}{\beta}x \pm \frac{\frac{2\sqrt{-\frac{1}{36\lambda\mu}}\alpha^3}{9}t\delta}{\beta^2}$.
2. The trigonometric function solution is	2. The trigonometric function solution is $u_{9,10}(x,t) = \frac{\alpha}{6}\sqrt{-\frac{6}{\beta}} \pm \frac{1}{6}\frac{\alpha\sqrt{-\frac{6}{\beta}}}{\sqrt{-\frac{1}{\lambda\mu}}\mu\sqrt{\frac{\lambda}{\mu}}tan\left(\sqrt{\lambda\mu}(\xi+C)\right)}$.

$v_3(x,t) = \frac{\rho\left(\pm\frac{1}{6\sqrt{(N^2+4\delta Q)}}\right)}{\tau\left(\pm\frac{1}{\sqrt{-(6N^2+24\delta Q)\tau}}\right)} - \frac{\left(\pm\frac{\delta\rho}{\sqrt{-(6N^2+24\delta Q)\tau}}\right)\sqrt{-\omega}tan\left(\frac{\sqrt{-\omega}\eta}{2M}\right)}{2\delta} + \frac{\rho}{12\tau\left(\pm\frac{1}{\sqrt{-(6N^2+24\delta Q)\tau}}\right)\sqrt{-\omega}tan\left(\frac{\sqrt{-\omega}\eta}{2M}\right)}.$	
3. The rational function solution is $v_5(x,t) = \frac{\rho\left(\pm\frac{1}{6\sqrt{(N^2+4\delta Q)}}\right)}{\tau\left(\pm\frac{1}{\sqrt{-(6N^2+24\delta Q)\tau}}\right)} + \frac{\pm\frac{\delta\rho}{\sqrt{-(6N^2+24\delta Q)\tau}}}{\eta} - \frac{\rho\eta}{24\delta\tau\left(\pm\frac{1}{\sqrt{-(6N^2+24\delta Q)\tau}}\right)}.$	

7.2. Comparative investigation of solutions to the nonlinear STFLGH model

Exact solutions of the nonlinear STFLGH equation have been extensively investigated owing to their significance in simulating nonlinear wave phenomena. Over the years, various analytical methods have been developed to analyze the dynamic behavior of this equation and to construct its exact traveling wave solution. Among these methods, Singh et al. [45] analyzed the nonlinear STFLGH equation via the Local Fractional Elzaki Variational Iteration Method (LFEVIM) to derive exact solutions in fractal Mittag-Leffler and hyperbolic forms, focusing on the pattern of ion-cyclotron waves for electrostatic potential expressed as a sequence of recurrence functions. In this study, the nonlinear STFLGH equation is analyzed by employing the generalized (G'/G)-expansion procedure. According to the outcomes presented in Table 2, this approach yields hyperbolic, trigonometric, and rational solutions, generating diverse wave patterns such as W-shape, singular soliton, smooth kink, anti-kink, bell-shape, flat parabolic, parabolic and compacton structures, which are portrayed through 3D, contour and 2D profiles. Additionally, linear stability analysis is conducted to confirm the stable nature of the obtained wave solutions. In comparison to the findings presented by Singh et al. [45], the obtained solutions exhibit a more diverse and richer wave structure. Consequently, this method extends

previous results and improves the analysis of nonlinear wave dynamics governed by the STFLGH equation.

Table 2: Comparison of the present outcomes with those of Singh et al.[45]

Outcomes derived in this study	Outcomes derived by Singh et al. [45]
1. The hyperbolic type outcome is $u_1(x,t) = \frac{\left(\pm\frac{1}{\sqrt{(N^2+4\delta Q)}}\right)k\sqrt{\omega}tanh\left(\frac{\sqrt{\omega}\eta}{2M}\right)}{2l} + \frac{k}{2\left(\pm\frac{1}{\sqrt{(N^2+4\delta Q)}}\right)l\sqrt{\omega}tanh\left(\frac{\sqrt{\omega}\eta}{2M}\right)}$, where $\eta = \frac{\mu}{\alpha}(x+\frac{1}{\Gamma(\alpha)})^{\alpha} - \frac{\lambda}{\alpha}(t+\frac{1}{\Gamma(\alpha)})^{\alpha}$, $\lambda = \pm\frac{\sqrt{-2(N^2+4\delta Q)\left(k^2M^2-((8\delta Q+2N^2)\mu^2)\right)}}{2(N^2+4\delta Q)}$, and μ is a constant.	1. The hyperbolic type outcome is $\aleph(\Lambda,\ell) = 2\sqrt{2}\mathrm{E}_{\mu}(-\Lambda^{\mu})\left(cosh_{\mu}(\ell^{\mu}) - \sqrt{2}sinh_{\mu}(\ell^{\mu})\right)$.
2. The trigonometric type outcome is $u_3(x,t) = -\frac{\left(\pm\frac{1}{\sqrt{(N^2+4\delta Q)}}\right)k\sqrt{-\omega}tan\left(\frac{\sqrt{-\omega}\eta}{2M}\right)}{2l} - \frac{k}{2\left(\pm\frac{1}{\sqrt{(N^2+4\delta Q)}}\right)l\sqrt{-\omega}tan\left(\frac{\sqrt{-\omega}\eta}{2M}\right)}$.	2. The Mittag Leffler type outcome is $\aleph(\Lambda,\ell) = 2\sqrt{2}\mathrm{E}_{\mu}(-\Lambda^{\mu})\sum_{k=0}^{\infty}(-1)^k\left(\sqrt{2}\right)^k\frac{\ell^{k\mu}}{\Gamma(k\mu+1)}$.
3. The rational type outcome is $u_5(x,t) = \frac{\left(\pm\frac{1}{\sqrt{(N^2+4\delta Q)}}\right)\delta k}{l\eta} + \frac{k\eta}{4\left(\pm\frac{1}{\sqrt{(N^2+4\delta Q)}}\right)\delta l}$.	

Thus, in this study, we investigated more distinct and generic wave structures than those identified by Singh et al. [45].

8. Conclusion

In this study, the nonlinear TFMK and STFLGH models have been analyzed using the new generalized (G'/G)-expansion method based on the beta derivative. This approach has successfully generated various exact analytical solutions of the equations, including hyperbolic, trigonometric, and rational forms. A comparative analysis with the results of previous studies has demonstrated the new wave structures which have never been extracted before in existing literature. The graphical depictions, including three-dimensional, contour,

and two-dimensional profiles have exhibited various physically significant solitary wave types, such as kink, anti-kink, singular soliton, compacton, bell-shape, W-shape, parabolic, flat parabolic, periodic and other soliton profiles. These representations have confirmed the validity of the mathematical results of the study and illustrated the influence of fractional parameters on wave behaviour. Moreover, linear stability analysis has been employed to gain insight into the system's behaviour under varying parameters. The obtained outcomes have contributed to further theoretical insights of nonlinear wave propagation in plasmas and higher-order dispersive media with memory effects, non-local phase transition dynamics in superconducting systems. In general, the suggested analytical framework has shown to be very strong and useful for obtaining exact solutions to numerous nonlinear fractional evolution equations. Furthermore, this approach is significant for other nonlinear models in the fields of engineering and mathematical physics. It might be applicable to other fractional nonlinear systems like the fractional Drinfeld-Sokolov-Wilson equation [46], the coupled Davey-Stewartson-Fokas system [47], and the Benjamin-Bona-Mahony-Peregrine equation [48] with power-law nonlinearity for future research to find new exact solutions and wave structures.

Author's Contributions Statement

Myder Jahan Proma: Investigation, Methodology, Validation, Visualization, Writing - original draft. Ripan Roy: Conceptualization, Investigation, Methodology, Validation, Visualization, Writing - original draft, Writing - review & editing. M. Ali Akbar: Conceptualization, Investigation, Software, Validation, Writing - review & editing. Wen-Xiu Ma: Formal analysis, Investigation, Supervision, Validation, Writing - review & editing.

Funding

No, this research did not receive funding.

Data Availability

All data generated or analysed during this study are included in this published article.

Declaration

Conflict of Interest

No, I declare that the authors have no competing interests.

References

[1] Wei L, Yang Y. Optimal order finite difference/local discontinuous Galerkin method for variable-order time-fractional diffusion equation. J. Comput. Appl. Math. 2021;383:113129.

[2] Boulaaras S, et al. Modeling the co-dynamics of vector-borne infections with the application of optimal control theory. Discrete Contin. Dyn. Syst. S. 2025;18(5):1331–52.

[3] Zhang Q, Zhou Y. Recent advances in non-Gaussian stochastic systems control theory and its applications. Int. J. Netw. Dyn. Intell. 2022:111–9.

[4] Bender CM, Hook DW. PT-symmetric quantum mechanics. Rev. Mod. Phys. 2024;96(4):045002.

[5] Sahu I, Jena SR. Numerical computation of fractional Kawahara and modified Kawahara equations in Caputo sense on integral transforms. J Supercomput. 2025;81(6):752.

[6] Zhang S, Zhang HQ. Fractional sub-equation method and its applications to nonlinear fractional PDEs. Phys. Lett. A. 2011;375(7):1069–73.

[7] Mamun AA, et al. Rational Sine-Gordon expansion method to analyze the dynamical behavior of the time-fractional phi-four and (2+1)-dimensional

CBS equations. Sci. Rep. 2024;14(1):9473.

[8] Gu M, et al. Explicit solutions of the generalized Kudryashov's equation with truncated M-fractional derivative. Sci. Rep. 2024;14(1):21714.

[9] Ma WX, Fuchssteiner B. Explicit and exact solutions to a Kolmogorov-Petrovskii-Piskunov equation. Int. J. Non-Linear Mechanics. 1996;31(3):329-38.

[10] Farhood AK, Mohammed OH. Homotopy perturbation method for solving time-fractional nonlinear variable-order delay partial differential equations. Partial Differ. Equ. Appl. Math. 2023;7:100513.

[11] Wang X, et al. Investigation of exact solutions of nonlinear evolution equations using unified method. Mathematics. 2022;10(16):2996.

[12] Ma WX, Lee JH. A transformed rational function method and exact solutions to the 3+ 1 dimensional Jimbo–Miwa equation. Chaos, Solitons & Fractals. 2009;42(3):1356-63.

[13] Rida SZ, et al. Residual power series scheme treatments for fractional Klein–Gordon problem arising in soliton theory. Sci. Rep. 2024;14(1):30596.

[14] Ma WX. Lump waves in a generalized Bogoyavlensky-Konopelchenko model with spatially balanced derivatives. Mathematics in Engineering. 2026;8(1):140-9.

[15] Kolebaje O, Popoola O. Assessment of the exact solutions of the space and time fractional Benjamin–Bona–Mahony equation via the (G'/G)-expansion method, modified simple equation method, and Liu's theorem. Int. Sch. Res. Not. 2014;2014(1):217184.

[16] Sahoo S, Ray SS, Abdou MA. New exact solutions for time-fractional Kaup–Kupershmidt equation using improved (G'/G)-expansion and extended (G'/G)-expansion methods. Alex. Eng. J. 2020;59(5):3105–10.

[17] Wu X, Xiong M, Guo Y. Analytic solutions for a (3+1)-dimensional extended shallow water wave equation in nonlinear phenomena. AIMS Math. 2025;10(8):18541–57.

[18] Roy R, et al. Bright–dark solitary wave solutions to the nonlinear fractional Boussinesq and breaking soliton equations. Nonlinear Dyn. 2025;113(8):8819–37.

[19] Podder A, et al. Dynamical behavior of soliton solutions to the space–time fractional combined KdV–mKdV equation through two robust techniques. Mod. Phys. Lett. B. 2025;39(18):2550031.

[20] Roy R, Akbar MA, Wazwaz AM. Exact wave solutions for the nonlinear time-fractional Sharma–Tasso–Olver equation and the fractional Klein–Gordon equation in mathematical physics. Opt. Quantum Electron. 2018; 50(1):25.

[21] Shahen NHM, et al. Solitary and rogue wave solutions to the conformable time fractional modified Kawahara equation in mathematical physics. Adv. Math. Phys. 2021;2021(1):6668092.

[22] Ma WX. N-soliton solutions and the Hirota conditions in (2+ 1)-dimensions. Optical and Quantum Electronics. 2020;52(12):511.

[23] Kawahara T. Oscillatory solitary waves in dispersive media. J. Phys. Soc. Jpn. 1972;33(1):260–4.

[24] Jin L. Application of variational iteration method and homotopy perturbation method to the modified Kawahara equation. Math. Comput. Model. 2009;49(3–4):573–8.

[25] Guner O, Atik H. Soliton solution of fractional-order nonlinear differential equations based on the exp-function method. Optik. 2016;127(20):10076-83.

[26] Topsakal M, et al. Exact solutions of some fractional differential equations by various expansion methods. InJournal of Physics: Conference Series 2016 (Vol. 766, No. 1, p. 012035). IOP Publishing.

[27] Bashar MH, Tahseen T, Shahen NH. Application of the advanced exp(-φ(ξ))-expansion method to nonlinear conformable time-fractional partial differential equations. 2021;13(1):68-80.

[28] Ullah I, et al. Single wave solutions of the fractional Landau–Ginzburg–Higgs equation in space–time with accuracy via the beta derivative and mEDAM approach. AIMS Math. 2025;10(1):672–93.

[29] Cyrot M. Ginzburg–Landau theory for superconductors. Rep. Prog. Phys. 1973;36(2):103.

[30] Zulqarnain RM, et al. Physically significant solitary wave solutions to the space–time fractional Landau–Ginsburg–Higgs equation via three consistent methods. Front. Phys. 2023;11:1205060.

[31] Roshid MM, et al. A variety of soliton solutions of time M-fractional nonlinear models via a unified technique. PLOS ONE. 2024;19(4):e0300321.

[32] Abdalla M, et al. Analysis modulation instability and parametric effect on soliton solutions for M-fractional Landau–Ginzburg–Higgs (LGH) equation through two analytic methods. Fractal Fract. 2025;9(3):154.

[33] Bukht Mehdi K, et al. Exploration of soliton dynamics and chaos in the Landau–Ginzburg–Higgs equation through extended

analytical approaches. J. Nonlinear Math. Phys. 2025;32(1):22.

[34] Ullah I, Shah K, Abdeljawad T. Study of traveling soliton and fronts phenomena in fractional Kolmogorov–Petrovskii–Piskunov equation. Phys. Scr. 2024;99(5):055259.

[35] Al Amin M, et al. Soliton solutions, bifurcations, and sensitivity analysis to the higher-order nonlinear fractional Schrödinger equation in optical fibers. Partial Differ. Equ. Appl. Math. 2025;13:101057.

[36] Atangana A, Oukouomi Noutchie SC. Model of break-bone fever via beta-derivatives. Biomed. Res. Int. 2014;2014(1):523159.

[37] Saad KM, Atangana A, Baleanu D. New fractional derivatives with non-singular kernel applied to the Burgers equation. Chaos. 2018;28(6):063109.

[38] Islam MA, et al. Stability analysis, bifurcation and chaotic dynamics, and analytical soliton solutions of the modified RLW-Burgers equation using an expansion scheme. AIP Adv. 2025;15(12):125214.

[39] Sagib M, Ghosh BP, Roy NC. New traveling wave solutions to the simplified modified Camassa–Holm equation and the Landau–Ginsburg–Higgs equation. Dhaka. Univ. J. Sci. 2024;72(1):7–13.

[40] Asghar U, et al. New exact soliton wave solutions appear in optical fibers with Sardar sub equation and new auxiliary equation techniques. Scientific Reports. 2025;15(1):4396.

[41] Teymuri Sindi C, Manafian J. Wave solutions for variants of the KdV–Burger and the K (n, n)–Burger equations by the generalized (G'/G)-expansion method. Math. Methods Appl. Sci. 2017;40(12):4350-63.

[42] Khan S, et al. Bifurcation, quasi-periodic, and chaotic analysis of the conformable fractional paraxial wave equation using the rational expansion method. AIP Adv.2025;15(5):055323.

[43] Islam A, Sagib M, Mamunur Rashid M, Al Amin M. Abundant optical soliton solutions to the fractional perturbed Chen–Lee–Liu equation with conformable derivative. Phys. Scr. 2024;99(5):055247.

[44] Shah NA, Dassios I, Chung JD. Numerical investigation of time-fractional equivalent width equations that describe hydromagnetic waves. Symmetry. 2021;13(3):418.

[45] Singh J, et al. A novel hybrid approach for local fractional Landau–Ginzburg–Higgs equation describing fractal heat flow in superconductors. Fractals. 2024;32(07n08):2440048.

[46] Noor S, et al. Investigating the dynamics of time-fractional Drinfeld–Sokolov–Wilson system through analytical solutions. Symmetry. 2023;15(3):703.

[47] Khan MA, et al. Soliton solutions of nonlinear coupled Davey–Stewartson Fokas system using modified auxiliary equation method and extended (G'/G^2)-expansion method. Scientific Reports. 2024;14(1):21949.

[48] Osman M, et al. Analytical study of solitons to Benjamin–Bona–Mahony–Peregrine equation with power law nonlinearity by using three methods. UPB. Sci. Bull. Ser. A. Appl. Math. Phys. 2018; 80:267–287.